2016

In-Cylinder Diagnostics Using Feedback from Resonant Cavity Ignition Sources

James F. Hunsucker III

In-Cylinder Diagnostics Using Feedback from Resonant Cavity Ignition Sources

James F. Hunsucker III, BSEE

Thesis submitted

to the Benjamin M. Statler College of Engineering
at West Virginia University
in partial fulfillment of the requirements for the degree of

Master of Science in
Mechanical Engineering

James E. Smith, Ph.D., Committee Chair
Roy Nutter, Ph.D.
Andrew Lowery, Ph.D.

Department of Mechanical Engineering

West Virginia University
Morgantown, West Virginia
2016

Keywords: Plasma ignition, in-cylinder diagnostics, resonator, QWCCR, engine, resonant frequency

Abstract

In-Cylinder Diagnostics Using Feedback from Resonant Cavity Ignition Sources

James F. Hunsucker III

The Quarter-Wave Coaxial Cavity Resonator (QWCCR) Plasma Igniter is a spark ignition replacement system based on a novel technology. This system creates coronal plasma through the use of radio frequency voltage step-up. Because this device is an open loop resonant structure, it is sensitive to changes in the environment it operates in, the physical and the combustion environment. A relationship can be developed between the effects of the pressure in the combustion environment and the changes in resonance frequency experienced by the igniter. These diagnostic capabilities can be utilized to detect and alleviate misfires, incomplete fuel burns, etc. in an engine cycle.

A series of tests were conducted to prove these principles. The QWCCR plasma igniter was inserted into the Cooperative Fuel Research (CFR) test engine. Data was collected via an in-cylinder pressure computer and a network analyzer. The engine was set at different increments in crank angle to map the changes in the parameters at different volumes throughout the compression and power strokes. During these tests there was no fuel or combustion only air as the medium in-cylinder.

The results compare a baseline frequency calculated from the in-cylinder pressure data and an experimental frequency that was collected using the network analyzer. The percent error between these two is at a maximum 1.725%. Three-dimensional plots were created from this data to show that frequency and pressure can be predicted and to show that this is a valid means of tracking changes in the combustion chamber. The results demonstrate that QWCCR Plasma igniter can be used as a diagnostics tool. This validation provides numerous additional opportunities for diagnostic capabilities using the other fundamental parameters of the igniter physical and electro-magnetic properties.

Tables of Contents

List of Figures

Nomenclature

Γ	reflection coefficient	N/A
ε_0	free-space permittivity	(F/m)
ε_r	relative permittivity	(F/m)
ε_{rN}	permittivity of gas/vapor under standard temperature and pressure	(F/m)
θ	temperature	(K)
θ_N	standard temperature	(K)
λ	wavelength	(m)
μ_0	free-space permeability	(H/m)
μ_r	relative permeability	(H/m)
ρ	material specific resistivity	(Ω/m)
ρ	magnitude of reflection coefficient	N/A
φ	phase	(°)
ω	angular frequency	(rads/s)
C	capacitance	(C)
c_0	speed of light	(m/s)
f	frequency	(Hz)
f_r	resonance frequency	(Hz)
J	joules	(J)
L	inductance	(H)
n	number of moles	(mol)
P	pressure	(bar, Pa)
P_f	time-varying forward power	(W)
P_N	standard pressure	(bar)

P_r	time-varying reflected power	(W)
R	gas constant	(J/K*mol)
R	resistance	(Ω)
R_0	standard resistance	(Ω)
SWR	standing wave ratio	N/A
SWR(f_0)	standing wave ratio at the operating frequency	N/A
v	velocity	(m/s)
V	volume	(m^3)
V_I	voltage of incident signal	(V)
V_R	voltage of reflected signal	(V)
VSWR	voltage standing wave ratio	N/A
X_C	impedance of capacitor	(Ω)
X_L	impedance of inductor	(Ω)
Z_I	impedance of incident signal	(Ω)
Z_R	impedance of reflected signal	(Ω)

Acknowledgments

There are many people I would like to thank that have helped to make this research a possibility.

I'd like to thank my advisor and committee chair Dr. James E. Smith for his support and constant push for my success and betterment. A great deal of opportunities have been presented to me because of my academic relationship with him. And for these I am very grateful. I feel that we have come to know each other quite well through this experience. We've come to know each other's strengths and weaknesses and how to overcome the latter. I look forward to continuing my education, in my pursuit for a doctorate, and my career under the direction of Dr. Smith.

I'd also like to thank Dr. Andrew Lowery. As office mates I often find myself looking to him for help and guidance. Drew's help in the setup, testing process, and data analysis of this research was invaluable. I look forward to working on many more projects with him in the future.

I also want to thank Dr. Roy S. Nutter. He was one of my professors during my undergraduate degree in electrical engineering. I've always found him to be a very helpful and intelligent individual. I look forward to a continued professional relationship.

I'd like to thank the Center for Alternative Fuels Engines and Emissions (CAFEE) for allowing me access to their CFR engine. Specifically I'd like to thank Ross Ryskamp and Jackson Wolfe. They both played pivotal roles in the testing process of this research. Jackson was there to run the CFR engine to allow the collection of data. And Ross was there to help answer my never ending stream of questions.

I'd also like to thank my partner in life, Nikole. We've been through so much together and I look forward to everything yet to come. You've helped get me through this whole process. I appreciated everything you do for me and us.

Finally, I'd like to thank my mom and dad. They have been the ever needed support to help me fulfill my dreams. I love you both dearly and do my best to make you proud.

Chapter 1: Introduction

The Quarter-Wave Coaxial Cavity Resonator (QWCCR) Plasma Igniter is a novel microwave plasma source replacement for a spark plug for internal combustion engines. [1] [2] [3] In a previous series of ignition tests at Wright Patterson Air Force Base this system was proven to provide faster and more complete combustion of unique gaseous mixtures than that of a standard spark ignition system. [4] The other important attribute of the QWCCR is its potential ability to act as a diagnostics tool. The fundamental aspect that allows for diagnostic capabilities is the physical and electro-magnetic characteristics of the coaxial cavity resonator.

In previous publications of this technology the system was primarily mentioned for ignition purposes. These publications did not adequately address the ability of this system to be used as a tool for in-cylinder engine sensing and diagnostics. In these internal combustion engine applications the coaxial cavity resonator is acting as an antenna and has the ability to probe the combustion chamber and react to changes in pressure, temperature, impedance, volume, etc. prior to combustion, during the entire combustion process, and after the coronal discharge has ceased. Since the QWCCR is a dynamic system, when used in an engine environment, this diagnostic information can be useful throughout the engine-cycle process.

The coaxial cavity resonator takes the form of a quarter wave structure. This allows it to be used as a step-up amplifying device to increase the electric field potential. The separating factor between this system and other coaxial cavity systems is these other systems are typically closed loop systems. The QWCCR is an open loop system allowing for it to be sensitive to the local environment. This allows the system to sense changes in pressure, temperature, etc. in the engine environment. All of these factors affect the operation and performance of the QWCCR. Small changes in the combustion environment will have a measureable effect on impedance and resonance frequency. Similarly, changes to the input of the resonator, such as frequency and power delivered, will affect the combustion process and diagnostic capabilities.

1.1: Research Objective: The objective of this research is to prove that the Quarter-Wave Coaxial Cavity Resonator Plasma Igniter can be used as an in-cylinder diagnostics tool by establishing a relationship between in-cylinder pressure and the resonant frequency that can be used to predict the events occurring in the combustion chamber.

1.2: Summary of Chapter 1

The QWCCR plasma igniter is an alternative to a spark plug in an ignition system. With the innate capability of being a resonator it is responsive to changes in its operational environment. These changes can be tracked and mapped to be used for diagnostic purposes. There is a relationship that can be shown that relates frequency and in-cylinder pressure. This dependent relationship is the bases for this research.

Chapter 2: Literature Review

This chapter is a literature review of the QWCCR Plasma Igniter and other resonator cavity ignition systems. It first goes through a basic introduction to spark ignition starting from the first spark plug. The next section goes into depth the QWCCR Plasma Igniter, how it works and what makes it unique for this diagnostics purpose. The following section reviews other resonator cavity ignition systems in order to show that this has not previously been tested as an aspect of other systems. These sections review patents and published works on these technologies. The last sections go through the science and equations relating to the operation of the QWCCR.

2.1: Introduction of Spark Ignition

Power is what moves things. Without the production of power there would be no electricity, automobiles, or air travel. The most abundant way of generating power is to burn or ignite a fuel source. These combustible fuels drive turbines for the creation of electricity or in the case of an automobile an internal combustion engine.

Fossil fuels are a concentrated organic compound. They are used to generate steam, electricity and power automobiles.

> Edwin Drake's successful extraction of oil at his well in northwestern Pennsylvania in 1859 marked the dawn of the age of petroleum. Petroleum's first decisive impact was displacing whale oil in lighting in the late 19th century. But it was the victory of the internal combustion engine over steam and electricity as the preferred means to propel the recently-invented automobile in the first decade of the 20th century that thrust petroleum into the prominence it still enjoys today. Fueled by gasoline made from inexpensive and readily available oil, internal combustion cars, notes Alan P. Loeb, "alone offered a combination of speed and power, range and infrastructure that gave motorists the ability to achieve the automotive purposes they desired." [5]

Fossil fuels are the most cost effective and abundant source of fuel creating power, available today. It is this reason that they are the most common fuel used to produce power. The energy released from burning fossil fuels is what is used to drive turbines and engines. In the case of turbines it is used to create steam, and in the case of engines it is used to drive pistons.

The spark plug is essential to providing the initial energy to ignite the fuel in spark-ignited engines. Edmond Berger invented the first spark plug, on February 2, 1839. Etienee Lenoir, however, was the first to use a spark plug in an internal combustion engine. Others creating early patents for spark plugs included Nikola Tesla (1898) [6], Frederick Richard Simms (1898) [7],

and Robert Bosch (1898) [8]. The spark plug has been in continuous use since its first inception, although the demand of its use has changed.

The automotive industry has been faced with the demanding task of satisfying new emissions standards. There are multiple ways that these issues are being addressed. The one that will be focused on in this review will deal with the spark ignition system. It is known, that currently with standard spark plugs, it is not possible to achieve complete combustion in most cylinder applications. Also the pollutants that are required to be eliminated, or minimized, include unburnt hydrocarbons, carbon monoxide (CO), nitrous oxides (NO_x), and sulfur oxide (SO_x). All of these pollutants are the result of combustion or the incomplete combustion of fuels.

In order to comply with these new emission standards spark plug manufacturers are attempting to modify or reinvent the spark plug to achieve maximum efficiency and improved combustion. These manufacturers are going about this in a number of ways, from focusing mainly on the modification of already existing spark plug designs to laser ignition and plasma ignition systems. It is these latter advanced technologies that this review will focus on.

For this experiment the engine used will be a four-stroke engine. This four-stroke process is comprised of the intake, compression, power, and exhaust cycles. Specifically this will focus on the compression and power strokes, these are centered on top-dead-center.

In order to verify the forthcoming results engine data from Zweiri is shown for the pressure in relation to crank angle. These results are from a single cylinder engine where top-dead-center is at 360°. [9]

The following graph shows the cylinder pressure in relation to crank angle, with top-dead-center in this case being at 360°.

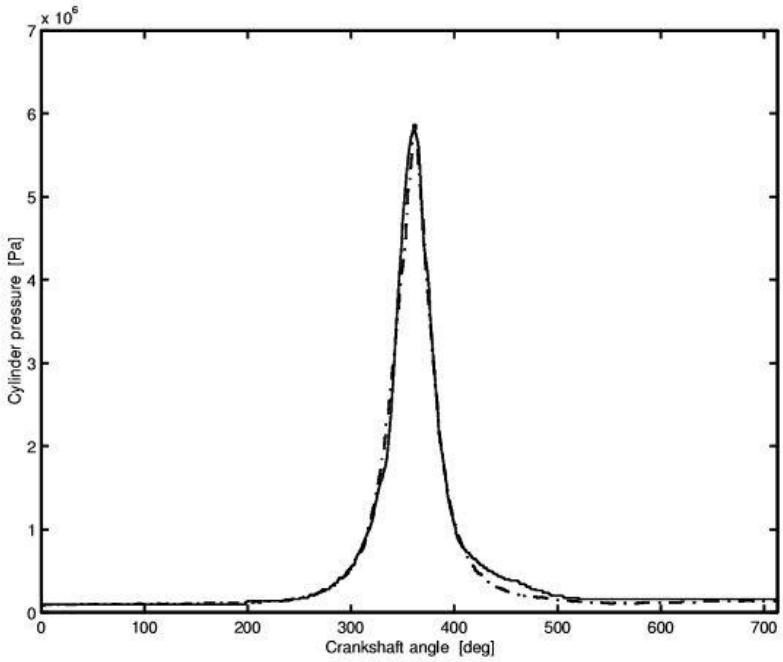

Figure 1: Cylinder Pressure (Pa) vs Crank Angle (degrees)

This is a typical pressure curve versus crank angle for a four-stroke engine during the compression and power strokes.

2.2: Review of QWCCR

The original patent for the QWCCR (U.S. 5,361,737, 08 November 1994) and documentation covered the invention of the apparatus of having a radio frequency oscillator, an amplifier, and a coaxial cavity resonator for the purpose of providing an ignition source to an internal combustion engine. The system is also adaptable for communication with the combustion chambers. The system provides a large plasma compared to that of a conventional spark plug. This plasma is created by using a radio frequency voltage and amplifying it, this is then resonated in the coaxial cavity in order to produce the plasma. [10] [11] [12]

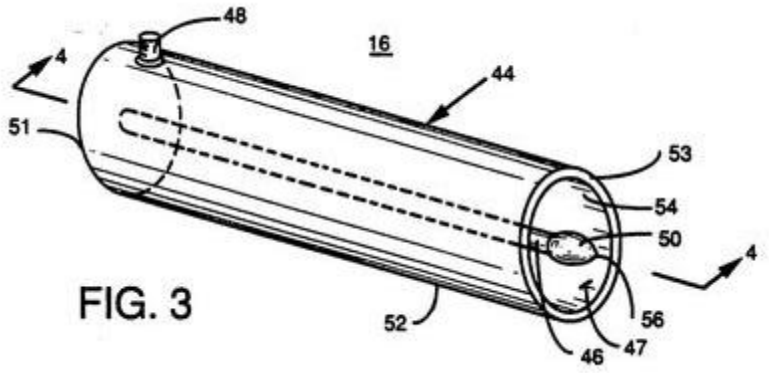

Figure 2: Figure 3 from US 5,361,737, Radio frequency coaxial cavity resonator as an ignition source and associated method [12]

Subsequent documentation follows the development of the plasma igniter in its adaption to a quarter-wave coaxial cavity resonator. This quarter-wave structure allows it to magnify the electric field. The testing for this device showed that it could operate under ambient conditions. [13] A model was made of this system at the 820-900 MHz frequency range. Further pressure testing showed that the device could generate plasma at the same operation pressures as a spark ignition system. [14] Based on the theoretical results from this model three identical igniters were created for engine testing. By testing these in an engine the optimal resonator geometry was determined and the first successful tests in an internal combustion engine were achieved in 2001. [15]

With successful testing several ways of improving the plasma igniter were developed. By adding a dielectric medium in the cavity with the correct dielectric properties the electromagnetic properties of the system could be modified. [16] [17]

From this point a feasibility analysis was conducted on the validity of this system to be used in Spark Ignition Engines. It was found that with some refinement it would be possible to provide the appropriate amount of energy necessary for automotive combustion purposes. [18]

Based upon prior testing and results a new patent (U.S. 7,721,697 B2, 25 May 2010) was created with this new knowledge of the system. [19] This patent covers the system more thoroughly describing in detail how the plasma is created from the radio frequency voltage and the coaxial cavity resonator. [19] A new high-level model of a pulsed microwave igniter is created based on the new designs. This model accounts for a simplistic plasma formation delay, a drop in resonance frequency as a result of plasma formation, and a subsequent change in the associated microwave reflection coefficient. Using this model a control system can be developed based on the variables. [20]

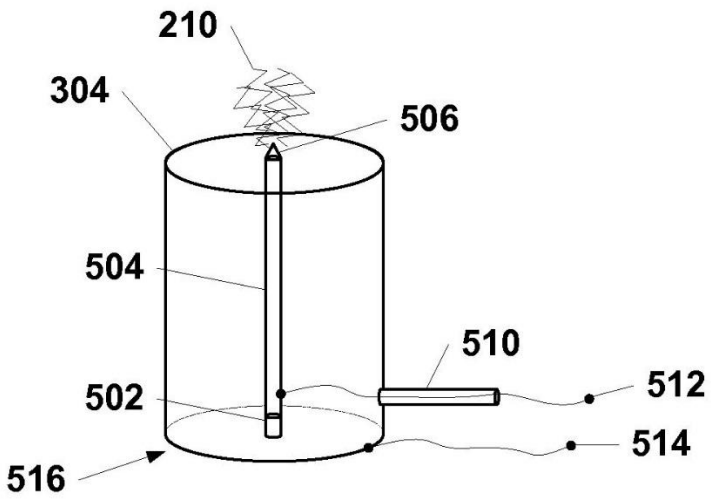

Figure 3: Diagram from U.S. 7,721,697 B2, 25 May 2010 of new form of apparatus [19]

Based on previous testing it has been shown that there is a significant environmental and economic benefit to using this system in an engine, because the system is able to operate at lean conditions. [4] The system also operates at a significantly lower energy requirement compared to that of a conventional spark ignition system. At 150 W, a microwave pulse of 2 ms can deliver energy of close to 300 mJ at a large sustained average power level compared to with a convention spark plug. [21] [22]

At this time, 2009, there is a focus on applying the technology to a new geometry that is capable of use in a Briggs and Stratton 16-hp V-twin engine. An analysis is done on the geometric and material parameters in order to adapt the system to this purpose for further testing. [22] This new prototype was used with a Briggs and Stratton engine with Jet A fuel. The Briggs and Stratton is a single cylinder engine with a fuel injection system. Tests were performed to determine the cold-start temperature limit, the lowest temperature the engine could be repeatedly started. [23]

Two more patents (US 8783220 B2, 22 Jul 2014, US 8887683 B2, 18 Nov 2014) were filed in order to protect new designs and methods of operation. A new folded cavity for the resonator is protected as this allows the system to operate at a lower frequency than the previously unfolded cavity. [24] [25] The new compact design was presented to show that the new folded cavity quality factors are comparable to the previously tapered cavity designs. [26] [27]

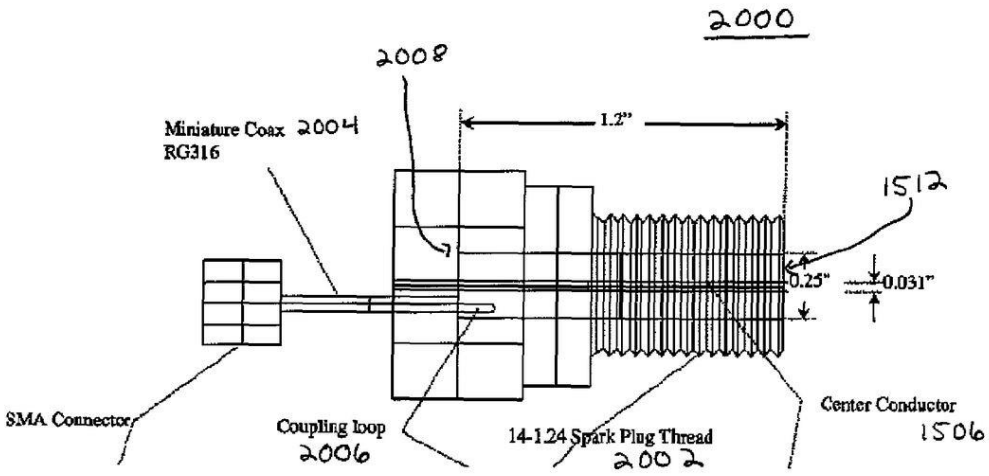

Figure 4: Diagram from US 8783220 B2, 22 Jul 2014, showing the component breakdown [24]

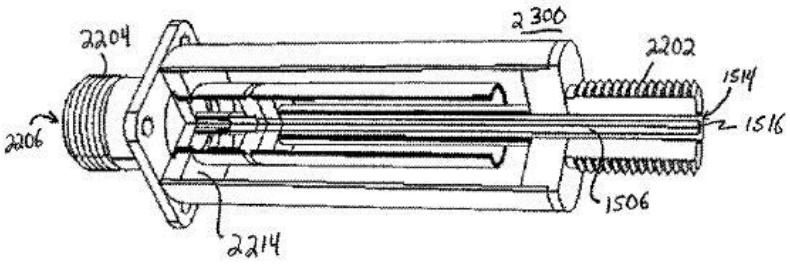

Figure 5: Diagram from US 8887683 B2, 18 Nov 2014, showing the folded cavity that permits the coaxial caivty resonator to resonate at a lower operating frequency than the unfolded varient [25]

The current iteration (US Patent 20150287574, 8 October 2015) of the plasma igniter involves the use of a dual signal. [28] This dual signal is composed of the radio frequency power source and a high voltage source that is used to step-up the total energy. This system allows the plasma igniter to operate at the mJ level since there is a minimal current present due to the nanosecond pulses. [28]

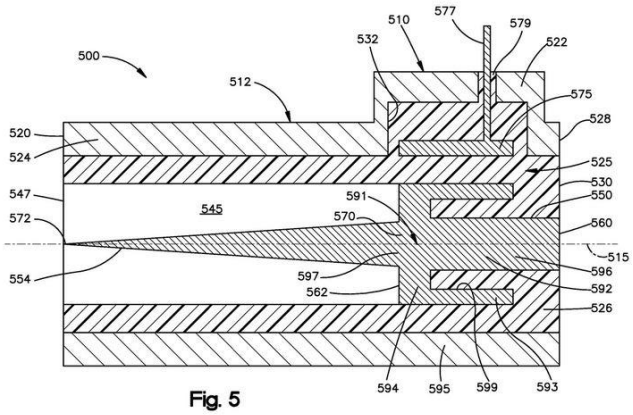

Figure 6: Diagram from US Patent 20150287574, 8 October 2015, showing the dual signal nature of the ignitor [28]

There is currently an active patent application concerning the diagnostics capabilities of this system. [29] This patent covers the use of the plasma igniter as an apparatus for igniting a combustible mixture that consists of a feedback module that is able to sense a condition in the combustion environment by measuring characteristics of the coaxial cavity resonator. This control is meant to process the feedback in order to modulate operation of the coaxial cavity resonator.

The version of the plasma igniter that was used for these experiments can be seen in Figure 6.

Figure 7: QWCCR Plasma Igniter

2.3: Review of Other Plasma Ignition Systems

The following are advanced ignition systems either in current development or production. This section will be a review of these systems and how they relate to this research.

System and method for generating and sustaining a corona electric discharge for igniting a combustible gaseous mixture

This system (US Patent 6883507, 26 Apr 2005) was developed by a company called Etatech. [30] The electric field in the combustion chamber is controlled such that the fuel-air mixture does not experience full dielectric breakdown producing a high current electric arc. This electric field is maintained high, but not high enough to cause complete dielectric breakdown. After the fuel-air mixture has been sufficiently ionized a flame front is developed to propagate throughout the chamber. This process is done by having a center electrode inside the combustion chamber being supplied by an electrical circuit that provides radio frequency power; a ground is established with the walls of the combustion chamber. This voltage differential produces a radio frequency electric field that causes the air-fuel mixture to ionize. [30] A control system (US Patent 8746218 B2, 10 June 2014, US Patent 20140226252, 14 August 2014) was also

developed separately for this system. The control system consists of measuring the baseline impedance of the circuit with the electrode, the measuring of an actual impedance circuit, the determination of an impedance set point based on the baseline impedance, a comparison of the actual impedance to the impedance set point, and the adjustment of the actual impedance based on the comparison of the actual impedance and the impedance set point. [31] [32] [33]

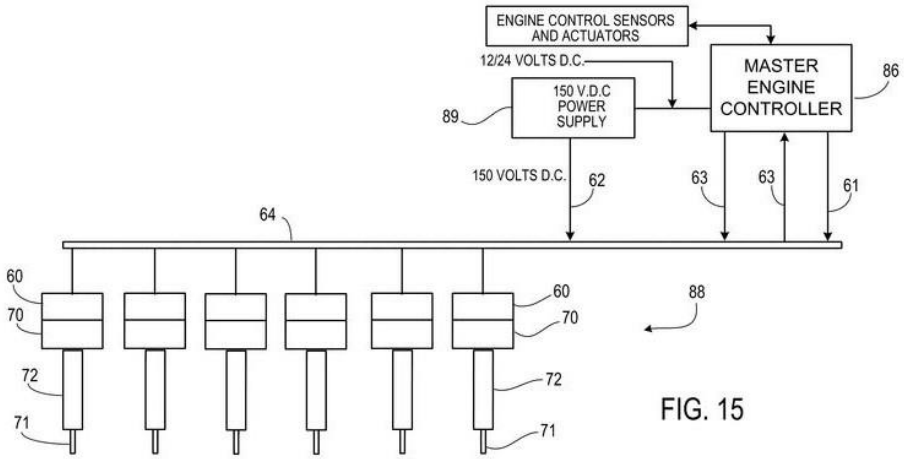

Figure 8: Diagram from US Patent 20140226252, 14 August 2014, showing how the control system would be established [31]

There is another related technology (US Patent 8217560 B2, 10 July 2012) developed by BorgWarner BERU developed by a different group. This technology is a corona ignition device for use in an internal combustion engine that consists of an ignition electrode, an outer conductor that surrounds the electrode, and an insulator between the electrode and outer conductor. The insulator and electrode protrude beyond the outer conductor. The electrode has a number of branches starting at its base. [34]

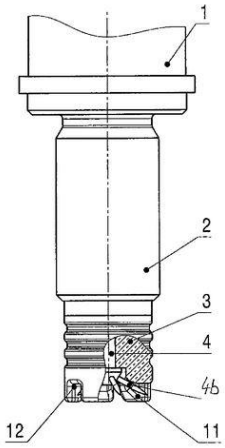

Figure 9: Diagram from US Patent 8217560 B2, 10 July 2012, showing the structure of the ignition device [34]

A high frequency ignition device was patented for use in an internal combustion engine (US Patent 20110146640 A1, 23 June 2011, US Patent 8550048 B2, 08 October 2013, US Patent 8767372 B2, 01 July 2014, US Patent 8860290 B2, 14 October 2014, US Patent 8857396 B2, 14 October 2014). The device consists of a center electrode, and insulating body around this center electrode, a metallic housing that has been threaded for insertion into an internal combustion engine, and an electrical circuit to provide HF excitation to the center electrode. The insulator is made of an electrically conductive coating. The HF for this system is to be at least one MHz and the voltage is to be a few kV. [35] [36] [37] [38] [39]

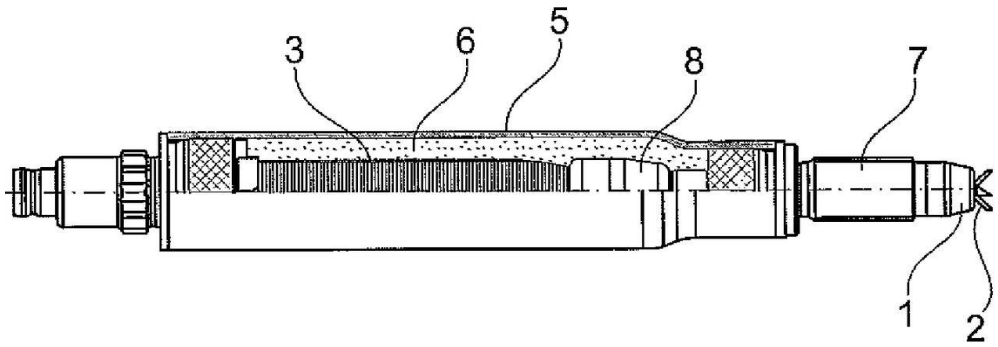

Figure 10: Diagram from US Patent 8767372 B2, 01 July 2014, showing the general structure and compenents that is outlined in the patent [34]

Ignition or plasma generation apparatus

This ignition system is designed to be installed without any modifications to the current engine system. [40] A plasma source is generated by a spark discharge; this is then expanded by radiating a microwave into the plasma. The way that this is generated causes a high electron temperature, but a low gas temperature. The frequency of the microwave is 2.45 GHz. This is

also the frequency of a magnetron from a microwave oven. A spark plug with an antenna was developed in order to adapt the system without changing the current engine system. This antenna is made of tungsten wire and goes around the center electrode. Plasma was successfully generated with this system up to 1.0 MPa. When this system was tested against a standard SI system it was shown to start combustion earlier. [40] At an IMEP of 275kPa, the plasma was able to increase the lean limit from 19.3 to 24.1. This system also reduced CO, CO_2, and NOx emissions as the airflow ratio was increased. This test was done in a single cylinder engine. [41]

This same system was then modified to be operable in a multi-cylinder engine system. This was done without modifying the combustion chamber. In order to adapt the system to be useable with a multi-cylinder system a mixer unit was developed. The mixer operated as a high-voltage and frequency isolator. The system once again showed improved initial combustion initiation. [42]

Patents (US Patent 8226901 B2, 24 July 2012, US Patent 20120258016 A1, 11 October 2012) were developed based on this technology. The first defines the system as having a center electrode that is supplied with energy from a spark discharge and microwaves in order to ignite an air-fuel mixture in an internal combustion chamber. This system includes the mixing circuit to combine the high-voltage pulse and the microwave energy, both of these coming from their respective generators. The nature of the mixing circuit causes the high-voltage pulse and the microwave energy to be superimposed upon each other on the same transmission line. [43] [44] The subsequent patent deals with the reflection of electromagnetic waves. The plasma generating device (U.S. application 20140041611) now includes an electromagnetic wave oscillator and a stub adjustment unit. The stub adjusts a short circuit location during engine operation based on the intensity of a reflected wave of the electromagnetic wave reflected from the antenna on the system. [45]

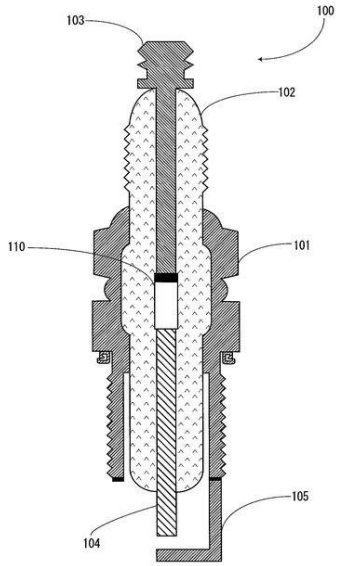

Figure 11: Diagram from US Patent 8226901 B2, 24 July 2012, showing general structure of ignition device [43]

Multi-event corona discharge ignition assembly and method of control and operation

This corona discharge fuel ignition system provides a corona discharge to ignite a fuel-air mixture with the purpose of reducing energy usage and costs compared to other corona discharge systems. The system consists of a power supply to provide radio frequency energy. The system uses pulses to provide the corona discharge. [46]

A corona discharge fuel igniter system and a control system for the long term operation of the system in a combustion environment were developed (US Patent 20120145136 A1, 14 June 2012). [46]The invention provides a corona discharge while incorporating the use of a specified insulator or dielectric material that increases the efficiency of the corona discharge in order to ignite fuel in a combustion environment. The dielectric material's purpose is to extend the life of the igniter system in a combustion environment. The igniter system uses radio frequency to produce the corona discharge. This RF voltage is passed through an electrical conductor to the tip of the igniter device. This conductor is surrounded by a ceramic dielectric material that provides efficiency to the corona discharge. The system also includes an inductor on the emission end of the igniter that increases the RF voltage. A dielectric material also surrounds this inductor. [47] In an attempt to suppress arc from forming when voltage is applied to the igniter various tip shapes were patented. Some of these shapes include angular depressions at the tip in multiple orientations. [48] A modification to the corona igniter's circuit was developed to add a self-tuning power amplifier. [49]

A subsequent patent (US Patent 8638540 B2, 28 January 2014) covers a corona igniter that is provided by a radio frequency electric field with the purpose to ionize a fuel-air mixture and create a corona discharge in the combustion chamber. This system consist of a housing, a coil

inside the housing to receive energy as a voltage and transmit this energy at a higher voltage, an electrode that is electrically coupled to the coil to receive the energy and provide the RF field, and a coil filler that consists of a resin material with the purpose of reducing capacitance. [50]

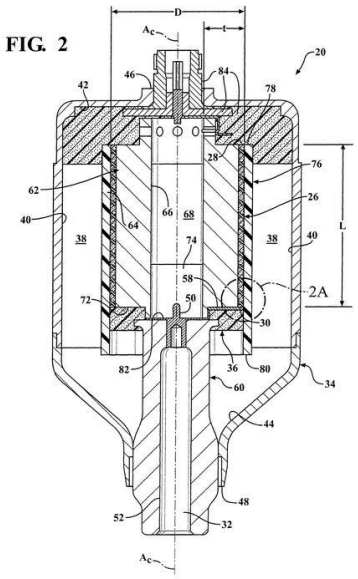

Figure 12: Diagram from US Patent 8638540 B2, 28 January 2014, showing the compnents of the corona igniter including the ignition coil [50]

The following patent (US Patent 8729782 B2, 20 May 2014) in the same series provides a corona ignition system that includes an electrode and insulator that extends along the electrode. [51]This electrode is formed from an electrically conductive material. The insulator contains a matrix of electrically insulating material on the firing end of the electrode. This insulator has the purpose of reducing and/or eliminating arcing during the use of the corona ignition system. The igniter creates controllable and repeatable non-thermal plasma that consists of multiple steams of ions in the form of a corona. This discharge is for the purpose of ignition of a fuel-air mixture with the benefits of improved fuel economy and reduced CO_2 emissions. [51]

The next patent in this series (US Patent 8749945 B2, 10 June 2014) builds upon and changes the parts of the previous system. [52] This system consists of an electrode, a corona drive circuit, and an energy storage circuit. This drive circuit provides energy to the electrode to emit a discharge from the electrode. The energy circuit provided is a supplementary system to the drive circuit; it stores energy while the drive circuit is providing energy to the electrode, and after a discharge is detected continues to provide energy in order to maintain the arc discharge being created. This continuous maintenance of the arc discharge is to ensure a robust and reliable ignition. [52]

A following patent (US Patent 8776751 B2, 15 July 2014) provides specifications for the emitting tip to enhance corona discharge. This enhanced tip could be a wire, layer, or sintered mass that is made of a precious metal. This emitting tip is placed upon a base member that is

made of a nickel alloy. The emitting member has a purpose of being more resistant to erosion and chemical corrosion than the base member. The emitting tip has a small spherical radius in order to concentrate and strengthen the electrical field that is emitted. [53]

Another patent (US Patent 8839752 B2, 23 September 2014) was made to provide this system with magnetic screening. This was achieved by including inductor windings between the housing, and an electric shield located between the housing and these inductor windings. The purpose of this was to prevent magnetic flux from emitting from the device. [54]

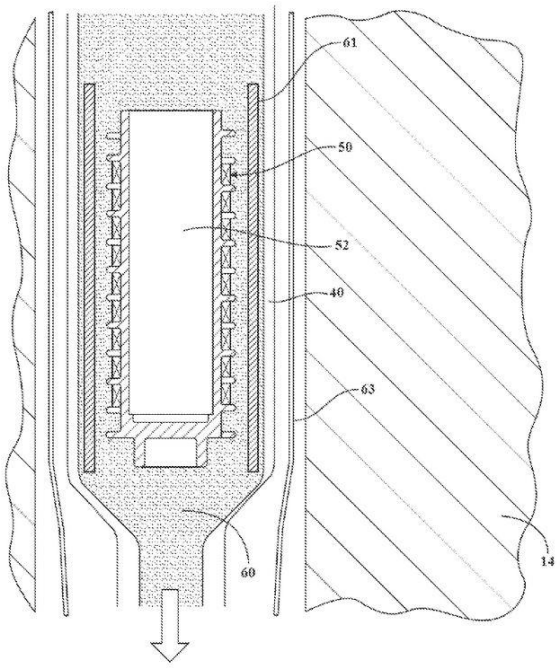

Figure 13: Diagram from US Patent 8839752 B2, 23 September 2014, showing the magnetic screening [54]

A patent (US Patent 8839753 B2, 23 September 2014) concerning the electrode gap further continues upon the structure of the corona igniter in this series. The center electrode is surrounded by an insulating material. There is a space between the electrode and the inner surface of the insulator that is the electrode gap. A shell of electrically conductive material is around the insulator. The space between the insulator and the shell is referred to as the shell gap. In either the electrode gap or the shell gap an electrically conductive coating is applied. These gaps and coatings are used to prevent ionized gas from forming and from a corona discharge being formed in these areas. The purpose is to ensure that a corona discharge is only created at the time of the ignition. [55]

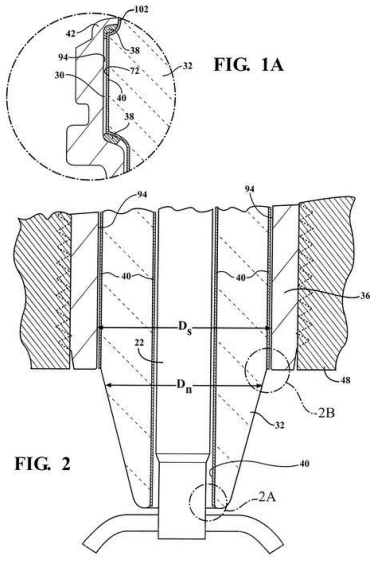

Figure 14: Diagram from US Patent 8839753 B2, 23 September 2014, showing the electrode gap [55]

A patent (US Patent 8844490 B2, 30 September 2014, US Patent 8749126 B2, 10 June 2014) was submitted changing this design to better control the location of the plasma, which consists of a wider shell gap. This wider shell gap is achieved by decreasing the thickness of the shell towards the emitting tip end of the corona igniter. This allows the flow of air into the shell gap. This process enhances the corona discharge along the insulator. [56] [57]

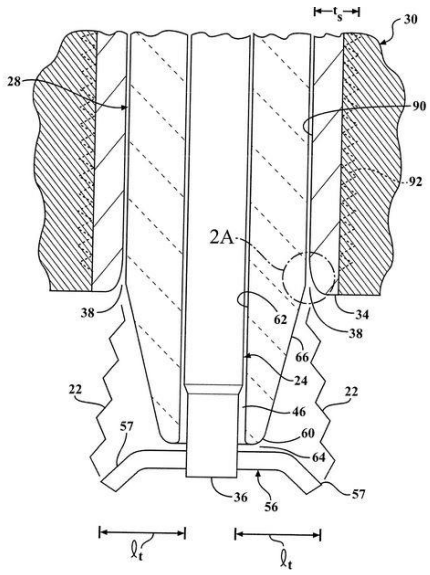

Figure 15: Diagram from US Patent 8844490 B2, 30 September 2014, showing the wider shell gap [56]

A patent (US Patent 9010294 B2, 21 April 2015) that further builds upon this design changes the electrode so that it consists of a core made of a material such as copper that is clad to another material such as nickel. This core material consists of at least 90% of the electrode.

The purpose of this modification is to reduce the temperature of the system. [58] This continues to build upon the series of patents in order to prevent the formation of a conductive path between the central electrode and the shell. This is done by adding an abruption extending radially from the center electrode. This abruption increases the thickness of the insulator. The abruption changes the electric field and voltage potential gradient in the shell gap, thus preventing the formation of a conductive path. [59]

Another adjustment to the system (US Patent 9088136 B2, 21 July 2015) was made in order to improve the electrical performance. This electrical performance was achieved by adding an intermediate conductive component between the outer conductive shell and the insulator. [60] An asymmetric firing tip is added to the system. This tip is noted by having one surface area with a sharp edge, and a second surface area having a rounded edge. This sharp area faces the fuel injector, while the round edge faces the cylinder block. This orientation makes it so the corona discharge is emitted from the sharp edge facing the fuel injector. This makes it so there is no arcing occurring between the tip and the cylinder block. [61]

None of these ignition systems provide in-cylinder diagnostics. There are also no currently available systems that can be used for combustion and provide in-cylinder diagnostics in a single system.

2.4: Resonators - Frequency, Temperature, Pressure

There is a fundamental principle in physics that links frequency, propagation velocity, and wavelength. [62] This can be expanded to compare the propagation velocity to that of light in a vacuum. This can further be expanded to include propagation through various mediums:

$$f_o\ [\mathrm{Hz}] = \frac{v\ [\mathrm{m/s}]}{\lambda\ [\mathrm{m}]} = \frac{v\ [\mathrm{m/s}]}{\lambda\ [\mathrm{m}]\sqrt{\mu_0\mu_r\varepsilon_0\varepsilon_r}} = \frac{c_0\ [\mathrm{m/s}]}{\lambda\ [\mathrm{m}]\sqrt{\mu_r\varepsilon_r}}, \quad (1)$$

where, f is the operating frequency, v is the wave velocity, λ is the wavelength, εr and ε_0 are the relative and free-space permittivity, respectively, and μ_r and μ_0 are the relative and free-space permeability, respectively, and c_0 is the speed of light in a vacuum.

This model assumes for the vacuum case that permittivity and permeability of the medium are fixed, time-invariant values. This is not true in an internal combustion engine, where the pressures and temperatures vary with respect to time and the varying positions of the piston, which is affected by the crank angle, in the cylinder during the combustion cycle. The permittivity can thus be modified so that it includes time-varying pressures and temperatures: [63]

$$\varepsilon_r(\theta, P, t) = 1 + \left[\varepsilon_{r_N}(\theta_N, P_N) - 1\right] \cdot \frac{\theta_N\ [\mathrm{K}] \cdot P(t)\ [\mathrm{bar}]}{\theta(t)\ [\mathrm{K}] \cdot P_N\ [\mathrm{bar}]}, \quad (2)$$

where, ε_r is the calculated permittivity, ε_{rN} is the permittivity of gas/vapor under standard temperature and pressure, θ and P are the process temperature and pressure, respectively, and θ_N and P_N are standard temperature and pressure.

Most gaseous fuels are non-magnetic, or in rare cases they are paramagnetic. In both of these cases the contribution towards μ_r is close to unity so for this study it will be assumed to be negligible.

This time varying model can be substituted into (1) in order to achieve a time-varying frequency that is dependent on the process temperature and pressure:

$$f_o(\theta, P, t) = \frac{c_0}{\lambda\sqrt{1 + \left[\varepsilon_{r_N} - 1\right] \cdot \frac{\theta_N \cdot P(t)}{\theta(t) \cdot P_N}}}, \quad (3)$$

The following figures were created using a Matlab code created by Dr. Andrew Lowery to show the change in temperature vs. operating frequency for a fixed pressure, P_N (1), and pressure vs. frequency for a fixed temperature, θ_N (2). [64] The third figure shows a surface curve of

temperature vs. pressure vs. frequency over the predicted operating conditions in a combustion environment.

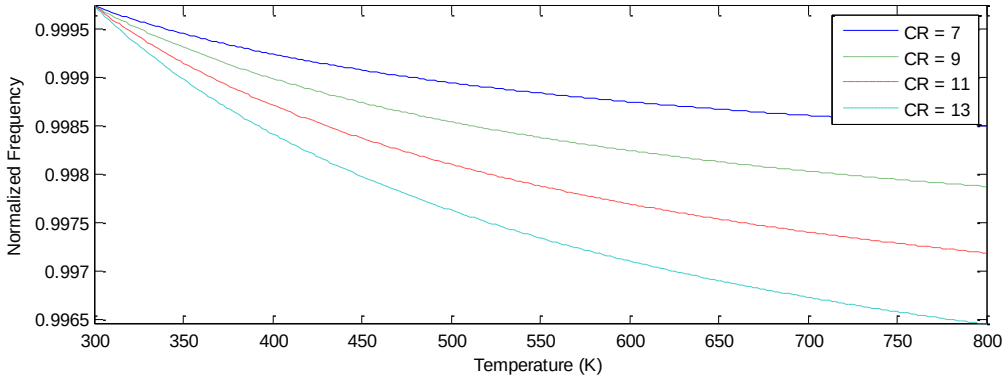

Figure 16: Example plot of temperature vs. normalized operating frequency [64]

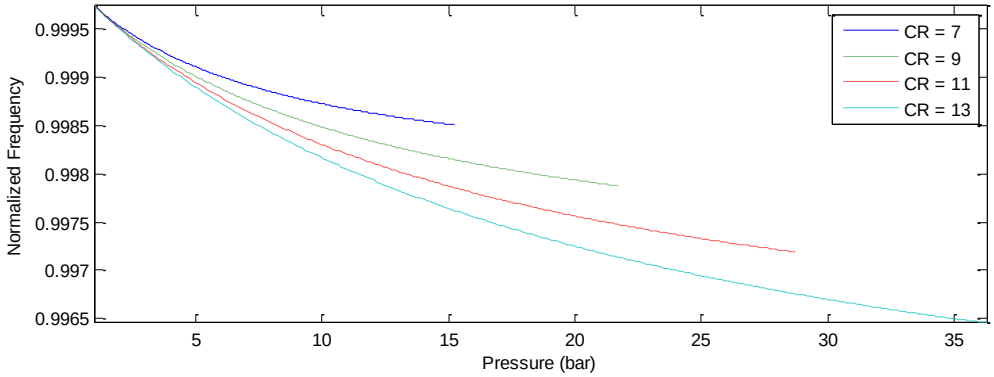

Figure 17: Example plot of pressure vs. normalized operating frequency [64]

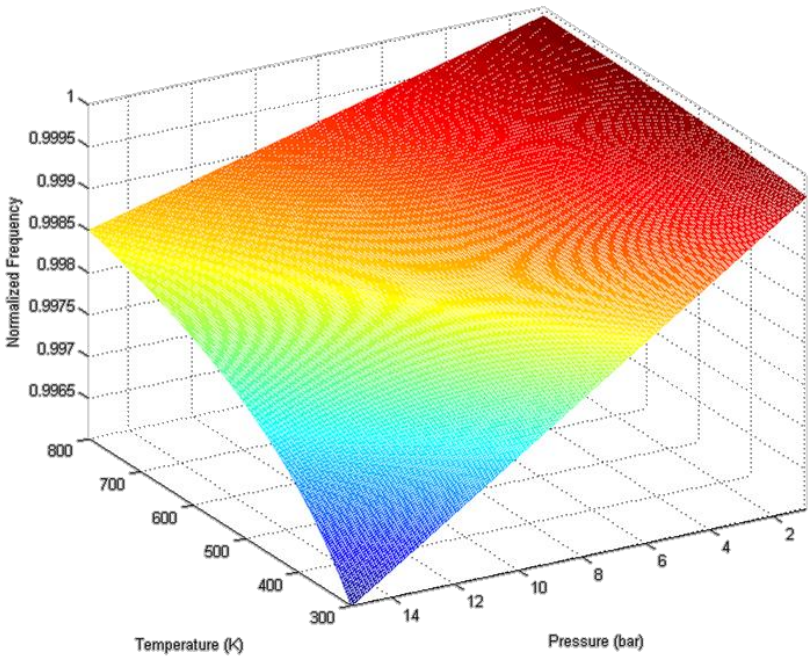

Figure 18: Example plot of temperature vs. pressure vs. normalized operating frequency [64]

It should be noted that continuity exists between all points of temperature and pressure. This demonstrates that knowing one data set, such as an initial set of conditions, the process can be tracked across the entire range of operation.

2.5: Summary of Chapter 2

Through reviewing the documentation on the QWCCR a better understanding of how the system works and where it is going in the future is established based on current patent applications. The transition to a dual signal plug allows for it to be operated at lower energies, because of the high voltage signal that is now being used to step up the radio frequency. This takes away the need for large power supplies and moves the system closer to being integrated into an engine. There is currently a provisional patent that is associated with covering the diagnostic capabilities of the QWCCR.

By reviewing other advanced ignition systems including plasma and corona, it can be shown that no other current technologies are utilizing a resonator device for diagnostic purposes. Some of these systems are utilizing the radio frequency power that the QWCCR uses. Because of this the systems should be able to create similar plasma to that of the QWCCR, but will not be able to do so at the same efficiency due to the lack of the dual signal, and more importantly not be able to operate at the high compression ratios of an internal combustion engine.

The QWCCR holds the unique advantage over all other in-cylinder diagnostics tools as it requires no additional modifications in order to perform diagnostics.

Chapter 3: Methodology

The following testing was completed in cooperation with the Center for Alternative Fuels Engines and Emissions (CAFEE) at West Virginia University. This testing was done in order to collect data to show the relationship of the pressure and temperature of the engine and the resonant frequency of the QWCCR with respect to the engines crank angle. The CFR engine was chosen for this process because it is a simple, single cylinder engine that the crank angle for data collection can be set. This was necessary to collect the frequency data as the sweep needed to be trigger to collect data only at the specified crank angle.

3.1: Testing Setup

The plasma ignition system was integrated into the spark plug port on the Cooperative Fuel Research (CFR) engine and connected to a HP 8753 network analyzer. The trigger from the in-cylinder pressure computer was imported into the network analyzer in order to sync the data collection. This trigger needed to be boosted in order for the network analyzer to properly receive the signal; this was done by running the signal through a signal generator in order to boost it. The plasma igniter was connected to the analyzer via an n-type cable.

The network analyzer was calibrated out to the n-type cable prior to testing using the n-type 50-ohm calibration kit.

Figure 19: CFR Engine

This figure shows the plasma igniter inserted into the spark plug port on the CFR engine.

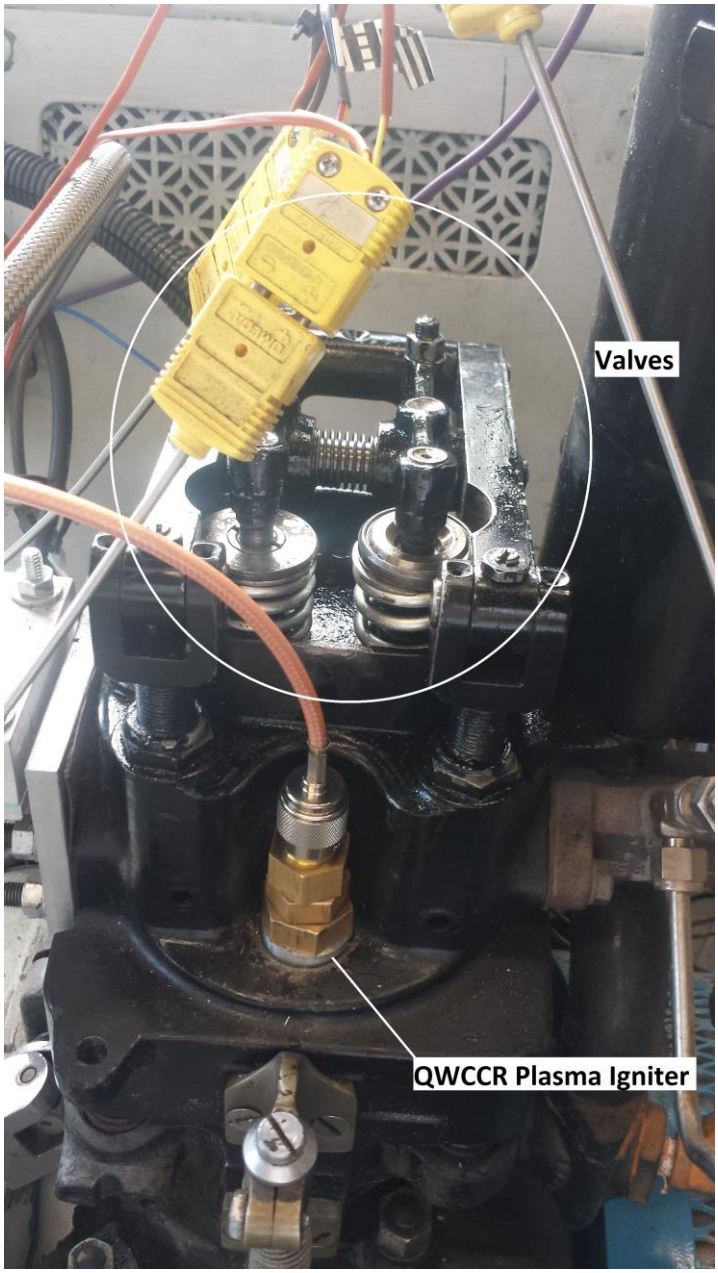

Figure 20: Plasma Igniter in CFR engine connected via n-type cable

This figure provides an up close view of the plasma igniter in the CFR engine. Also in this picture a closer view of the valves has been provided.

Figure 21: Network analyzer, signal generator, and oscilloscope

This figure shows the other components in the test set up consisting of the Tektronix TDS 3012B two channel color digital phosphor oscilloscope, the Global Specialties 4001: 5 MHZ ultra-

variable pulse generator, that is being used as a trigger, and the HP 8753 network analyzer that the plasma igniter is connected to via the n-type cable.

3.2: Testing Process

In order to collect the needed data a data logger was used to collect the engine data and the network analyzer was used to collect the frequency data. The network analyzer was set to collect data at the desired crank angle set by the computer. It was able to collect these specific points because of the syncing of the triggers.

The data collection consisted of setting up the system as shown, setting the crank angle with the computer, and then having the analyzer perform a sweep. The network analyzer data collection settings were set prior to testing. The range of the sweep was between 2.39 - 2.53 GHz. This range was chosen because prior to this test the plug was examined using the network analyzer and this range covered the curve of the plug. The resolution used for this sweep was 201 data points. The sweep was saved as a data file onto a floppy disk. This data was then later imported into a Matlab file for processing.

The engine was set to run at approximately 500 RPM, with a compression ratio of 5:1. For the purposes of this validation testing no fuel was used in this test. All of the data collection was done with air as the only intake.

The data logger collected data throughout the entire testing process. This consisted of pressure, intake and outtake temperatures, and engine speed. The pressure data was collected from a piezoelectric sensor in the cylinder. [65]

The specific crank angles that were used for data collection were from -180° to 180° at 10° increments. This range of angles was chosen because they cover the range of the valves being closed. The compression process exhibits an almost sinusoidal structure, so the incrementation of the crank angle of 10° is suited because this sinusoidal nature and be properly observed with this resolution. This 10° incrementation provides a good handoff for data collection timing. In a fully implemented system the positions at which are sample could be set to certain degrees that show diagnostic significance or based on timing. This range and incrementation shows the minimums and maximums as well as showing the full broad spectrum.

These angles coincide with the compression and power stroke of the engine. Power stroke is an interesting range to have diagnostic capabilities. During the power stroke misfires and the completeness of fuel combustion can be observed.

All the data collected was in the form of data files that could be imported into spreadsheets.

3.3: Data Processing

A Matlab file was used to calculate the volume of the cylinder based upon the crank angle and geometry of the engine cylinder. This can be found in appendices A:2.

The data collected from the data logger was in the form of text files, however, they were encrypted and needed to be decrypted with the use of a Matlab file, which can be found in appendices A:1. Data received from this file includes: engine speed, intake and exhaust temperatures, cylinder pressure, average temperature, and maximum temperature.

From the data logger in-cylinder pressure at the individual crank angles is determined. Intake and outtake temperature are included in the data collection, however, it is in-cylinder temperature that is desired. In order to calculate this in-cylinder temperature the ideal gas law equation was used:

$$PV = nRT, \tag{15}$$

where, P is the pressure in Pascal's, V is the volume in m^3, n is the amount of the substance of gas in moles, R is the ideal gas constant, and T is the temperature of the gas in kelvin

The pressure at each crank angle is used, along with the volume at the crank angle. The gas constant R is given as 8314 J/K*mol. In order to find the amount of moles (n) the pressure at atmospheric, the volume at -180°, the gas constant, and the average intake temperature were used. These parameters were chosen as this would determine the amount of air in the cylinder for the testing process. The elevation in Morgantown, WV is 961 ft., this gives a local atmospheric pressure of 97855.31426 Pa. The average intake temperature was 288.6613419 K. The n calculated ($2.73E^{-5}$ mol) was considered to be constant, as the amount of gas in the cylinder would not change for this experiment as there was no combustion present. This was deemed to be a good starting point for diagnostics in an ideal situation as there was to be no combustion. And this takes in the assumption that the valves do not leak holding the moles of the gas to be constant.

After establishing the constants n and R, the temperature was calculated at each crank angle from the pressure at each crank angle and the volume of each crank angle.

A baseline was created for pressure from this data. The average at each crank angle was used for this baseline.
From this pressure and calculated temperature the frequency could be calculated. The following equation shown early as (Equation 3) was used:

$$f_o(\theta, P, t) = \frac{c_0}{\lambda\sqrt{1 + \left[\varepsilon_{r_N} - 1\right] \cdot \frac{\theta_N \cdot P(t)}{\theta(t) \cdot P_N}}}, \tag{16}$$

The speed of light is 299792458 m/s which was used for c_0. The wavelength was calculated based upon the resonant frequency previously determined with the network analyzer, this value was 2.45 GHz. The resulting wavelength was 0.122364268571429 m. The dielectric constant for air is 1.00059 S/m. The sub n components represent standard conditions, in this case the initial conditions used for the calculation of n were used, intake temperature and the air pressure (bar) at elevation. The sub t components represent the experimental pressure and temperature.

This equation allows for the calculation of frequency from the in-cylinder pressure previously found. This data was also calculated for every crank angle allowing for the establishment of a frequency baseline. These data sets and baseline are plotted along with the frequency data collected from the network analyzer in the following results section.

From the pressure data the density can also be found by modifying the ideal gas law equation:

$$\rho_{baseline} = \frac{P}{R * T}, \tag{17}$$

The frequency data from the network analyzer was also in the form of text files. These individual files for each crank angle were imported into excel and combined. The data is initially imported as SWR. The minimum SWR is used to find the resonant frequency for each sweep.

The data from the baseline was compared to that of the experimental frequency to calculate percent error:

$$\%\ error = \left|\frac{\#_{experimental} - \#_{baseline}}{\#_{baseline}}\right| * 100, \tag{18}$$

Once again using a previous equation (Equation 3) the relationship between pressure and frequency can be explored to find experimental density:

$$f_o(\theta, P, t) = \frac{c_0}{\lambda\sqrt{1 + \left[\varepsilon_{r_N} - 1\right] \cdot \frac{\theta_N \cdot P(t)}{\theta(t) \cdot P_N}}}, \tag{19}$$

The same initial parameters are used as were used in calculating the frequency from the pressure data. The ratio of $\frac{P(t)}{\theta(t)}$ is found so that it can be used to find the experimental density.

$$\rho_{experimental} = \frac{P(t)}{\theta(t)} * \frac{1}{R}, \tag{18}$$

With the baseline pressure, baseline frequency, crank angle, and experimental frequency a 3-D plot can be created.

3.4: Summary of Chapter 3

This section showed the experimental setup, data collection process, and how the data was processed. The setup consisted of the CFR engine, the QWCCR Plasma Igniter, and the equipment needed to collect the data including the data logger and the network analyzer. The collection process explains how the crank angle was set with the computer allowing the network analyzer to perform a sweep at each individual crank angle. The data processing section walks through all the information necessary to process the data into useful information, including the values for specific variables and equations used. From this data plots were created to display the results, which can be seen in the following section.

Chapter 4: Results

In this chapter the results will be discussed in detail. A baseline was established for pressure, temperature, and frequency from the data in order to show the consistency of the data collected. Percent error is calculated by comparing the results from individual data runs versus this baseline. The final portion of this chapter will present graphs from another study that tracked similar results for pressure and temperature in relation to crank angle. [9]

4.1: Results Compared to Baseline and Percent Error

The object of this study was to establish a connection between the parameters of an engine and the resonance frequency across the crank angles of the engine.

This first plot (Figure 21) shows the change in pressure with respect to crank angle that was collected from the data logger.

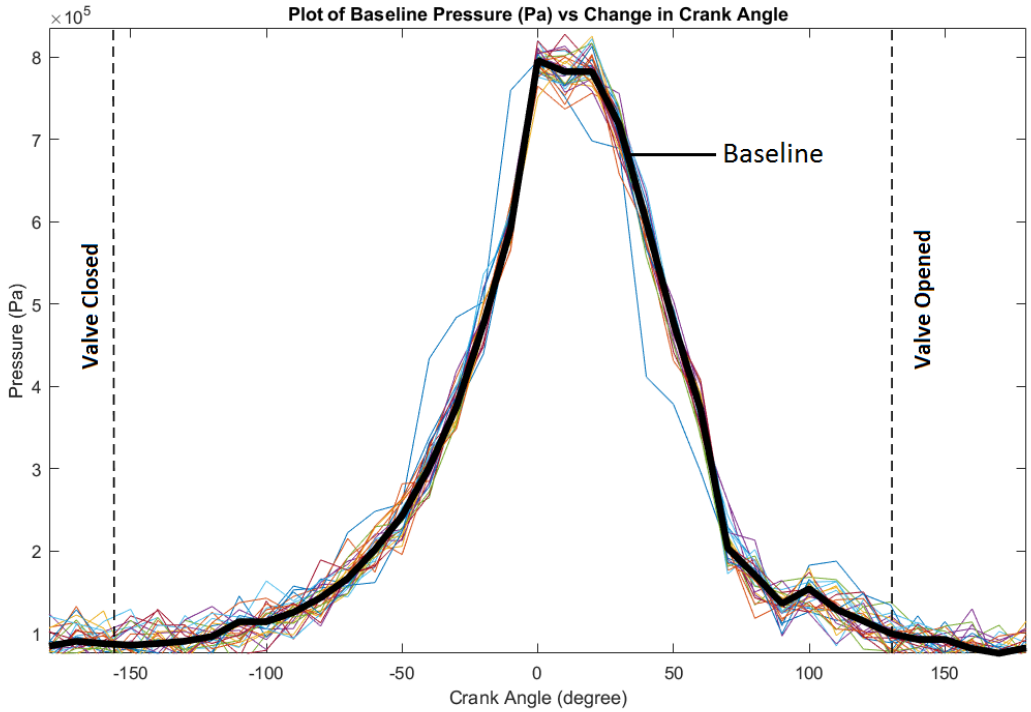

Figure 22: Plot of Baseline Pressure (Pa) vs Change in Crank Angle

The established baseline is shown in black. The two vertical dashed lines show the crank angles where the valves close and open, -156.5 and 130.5. Data outside these lines is susceptible to error, as the cylinder is not fully sealed. The dip at the peak of the pressure curve can also be explained by these valves. This CFR engine is an older system, and its age, wear and tear can be shown by the valves leaking at the peak pressure.

This next plot (Figure 23) shows the frequency calculated from the pressure the frequency collected from the network analyzer.

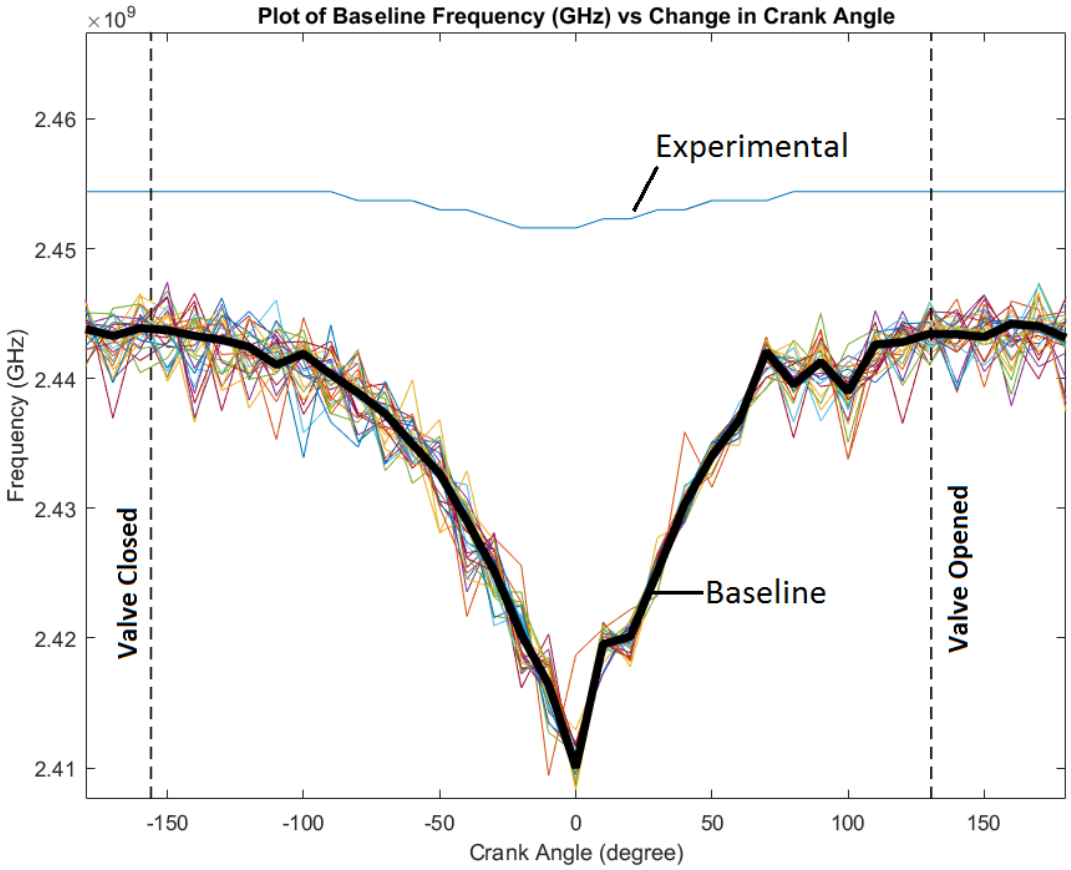

Figure 23: Plot of Baseline Frequency and Resonant Frequency from network analyzer vs Change in Crank Angle

The baseline frequency calculated from the pressure data is shown in black. The frequency from the network analyzer is shown as the blue line. The frequency collected from the network analyzer was found to be discretized, this is due to the number of points selected for the sweep on the network analyzer. This could be improved by increasing the number of points in the sweep.

The next plot (Figure 24) shows that based on the pressure a frequency can be found that is at all points less than 1.725% error of the resonant frequency found with the network analyzer. However this does not tell the whole story, because of the need to take into account the resonator properties. These two curves do not fall within a 3 dB bandwidth. This difference would not allow the QWCCR to operate properly; it could not achieve the conditions necessary for ignition.

There is a clear offset between the two curves of approximately 10 MHz. Using this method it can be shown that the resonance frequency can be found during this portion of the engine cycle. Things that cannot be found are the 3 dB bandwidth, the Q, SWR, and the various power measurements.

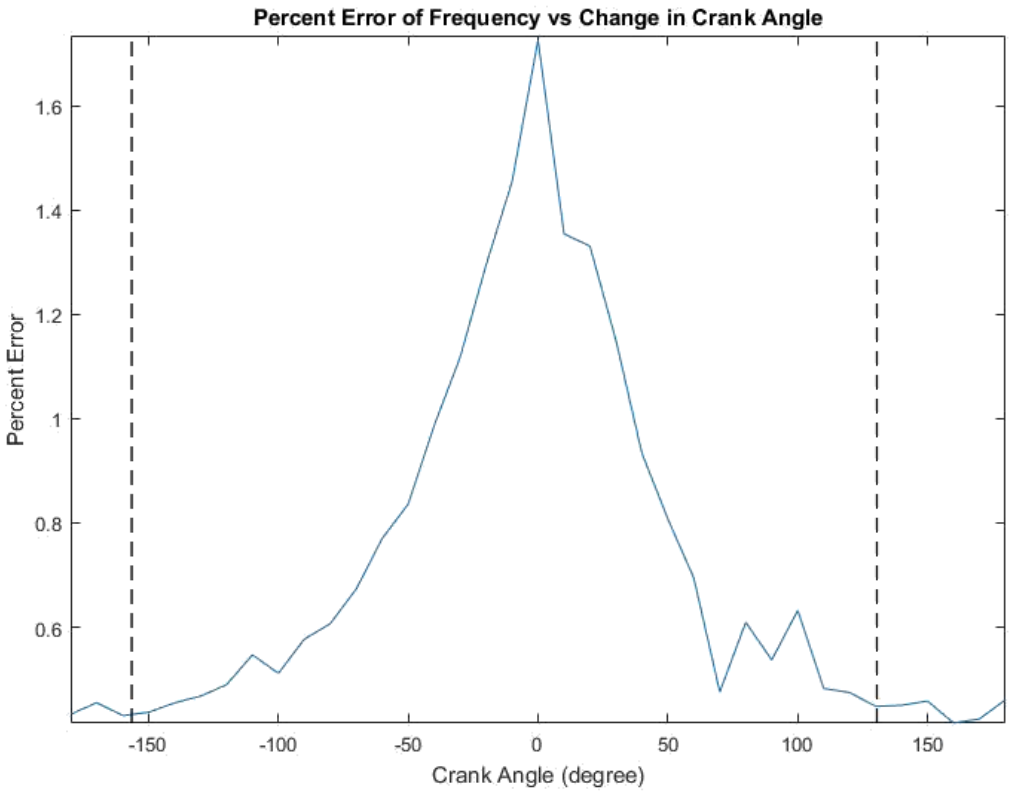

Figure 24: Percent error between experimental frequency and baseline frequency

The next plot (Figure 25) shows the density calculated from the pressure and the density calculated from the frequency found by the network analyzer.

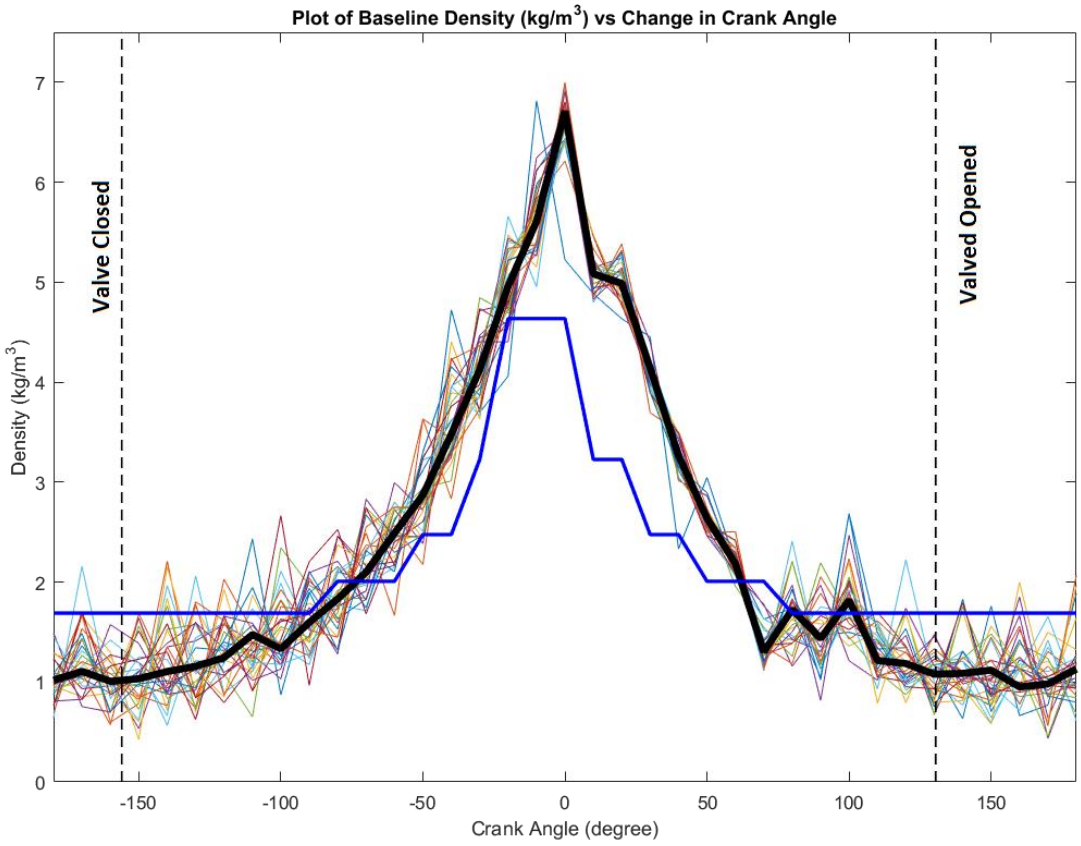

Figure 25: Plot of baseline density and density calculated from the frequency

The baseline density from the pressure is shown in black. The density from the frequency is shown as the blue line. The density from the frequency shows the same discretizion that was found in the frequency from the network analyzer. This could be fixed in the same way as the frequency by increasing the number of points in the sweep.

The next plot (Figure 26) shows the percent error for the experimental density and baseline density:

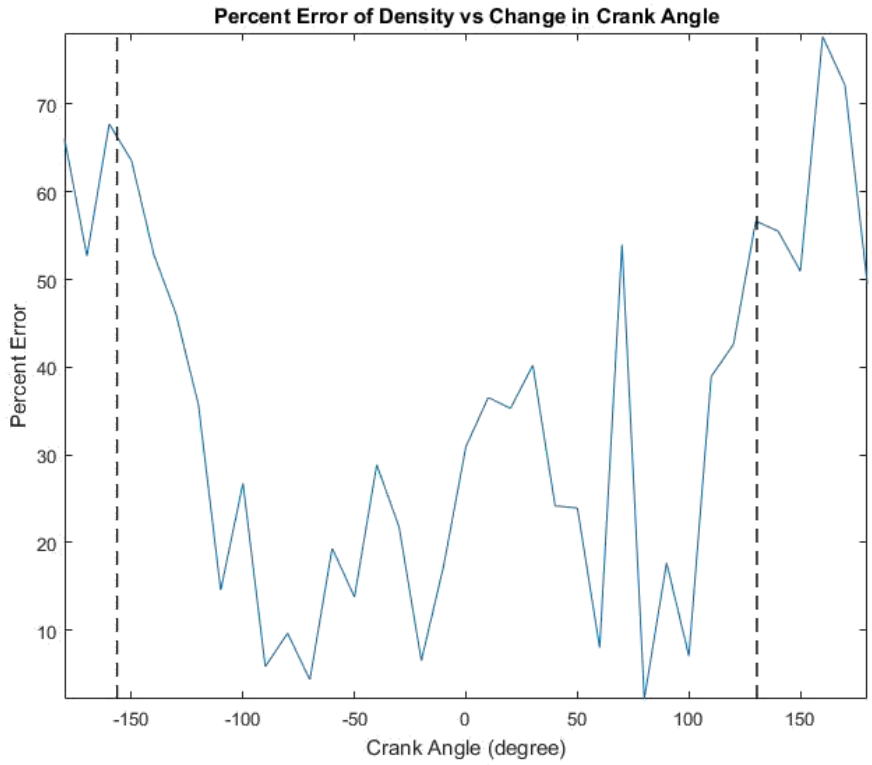

Figure 26: Percent error between experimental density and baseline density

The error at the trailing ends and the top near top dead center of the density are due to the resolution as can be seen in the density plot (Figure 25).

The following table lists the percent error for the frequency and the density. The ranges outside of -150° and 130° are taken out of the error analysis because the system is no longer a closed loop system since the valves are open. The error at top-dead-center is artificially large due to the leaks at maximum pressure and the age of the engine. The error in the range of 60°-100° is due to mechanical linkage slop in the piston motion.

Percent Error	Minimum	Maximum	Average
Frequency	0.437031741%	1.725585583%	0.789007832%
Density	2.142010431%	63.56411371%	27.07050832%

The following two 3-D plots (Figure 27 and Figure 28) show the 3-D relationships between pressure, frequency, and crank angle and density, frequency, and crank angle.

This first plot (Figure 27) shows both the baseline pressure and baseline frequency versus the crank angle of the engine and the baseline pressure and experimental frequency versus the crank angle. This 3-D plot provides a combine view of the two that allows for a comparison. Following what was previously stated with the individual plots as the pressure reaches the maximum at crank angle 0° the observed frequency changes.

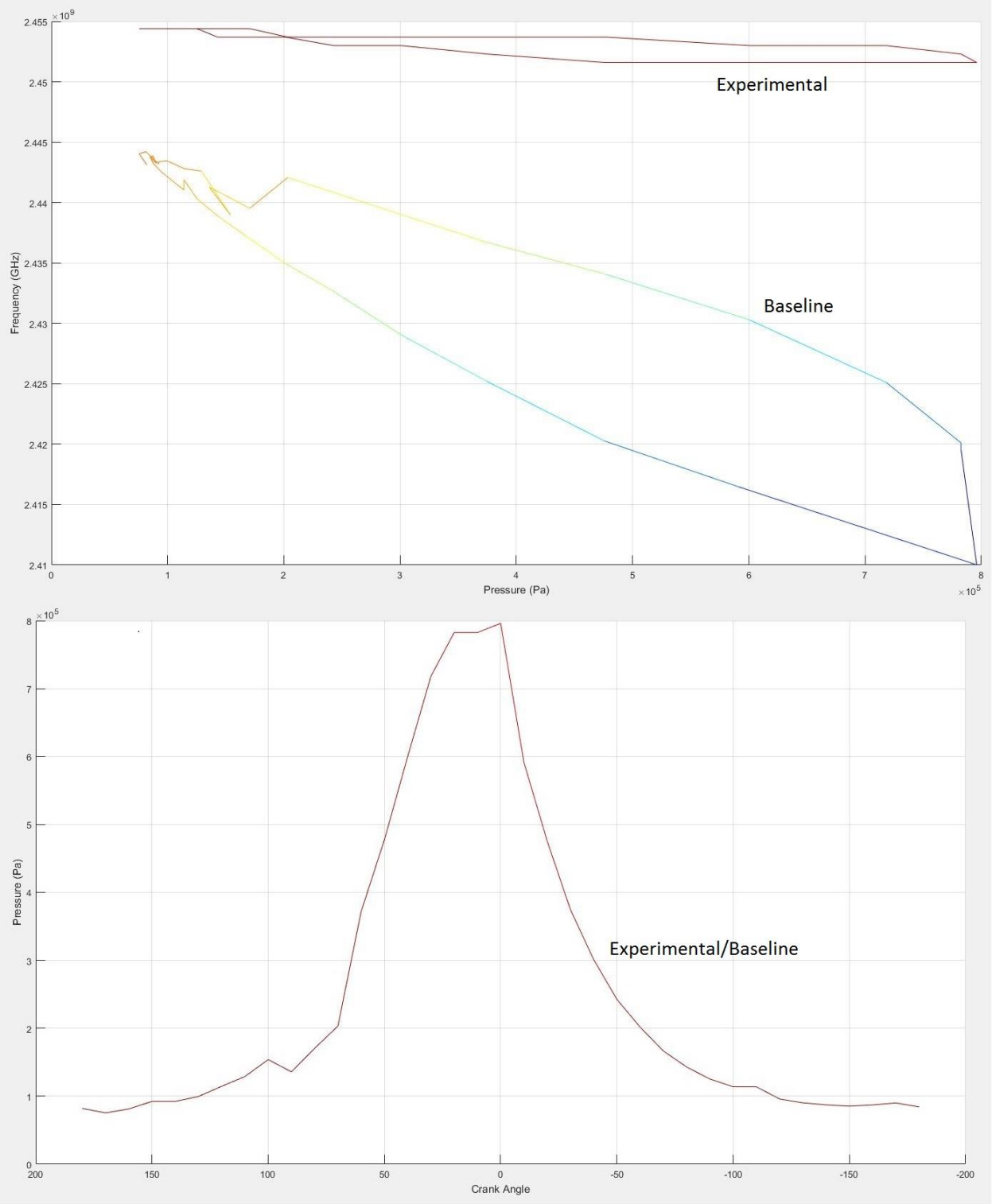

Figure 27: Plot of Baseline Pressure and Baseline Frequency, and Baseline Pressure and Experimental Frequency vs Crank Angle

It can be seen that there is a relationship that can be traced between pressure and frequency.

The next plot (Figure 28) shows both the baseline density and baseline frequency versus the crank angle of the engine and the experimental density and experimental frequency versus the crank angle. The experimental density shows the same discretizion shown previously with the density plot (Figure 25).

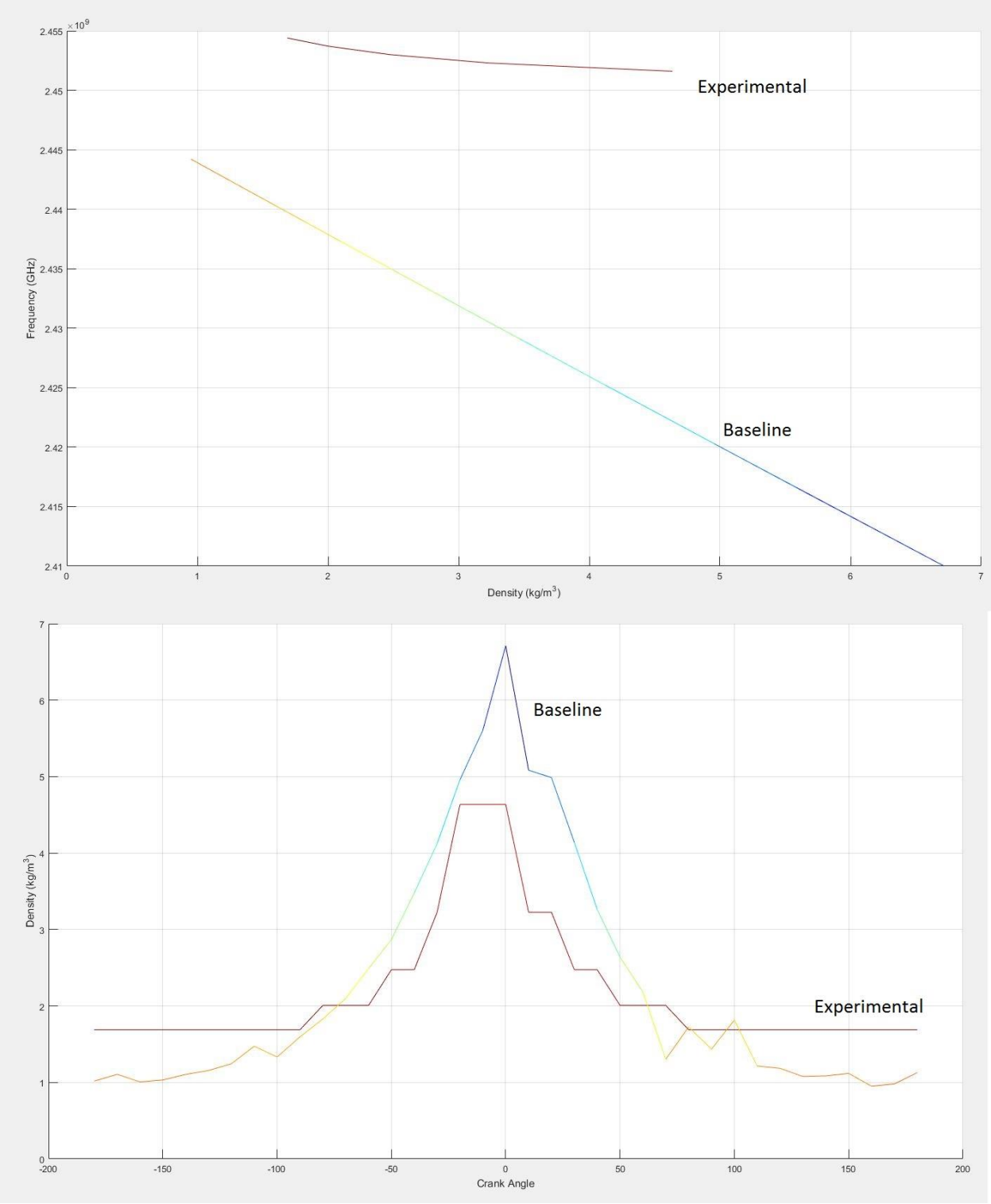

Figure 28: Plot of Baseline Density and Baseline Frequency, and Experimental Density and Experimental Frequency vs Crank Angle

As seen previously with Figure 26 the relationship between density and frequency can be used to trace the events occurring in the cylinder.

4.2: Summary of Chapter 4

This chapter went through the results calculated from the raw data. It displays the pressure and frequency curves with respect to the crank angle. The baseline frequency was calculated from the in-cylinder pressure data. This calculated frequency is then compared to the experimental frequency collected from the network analyzer. The percent error between these two is at a maximum approximately 1.725% throughout the crank angles. From both of these sets of data a density can be found. A baseline density was calculated from the in-cylinder pressure and the experimental density was calculated from the experimental frequency. From these densities the percent error was calculated. The average percent error for the density is approximately 27.07%. Three-dimensional plots were created from this data in order to show how two elements can be traced together against the crank angle of the engine.

By comparing frequency plots it is shown that frequency and pressure can be predicted and that this is a valid means of tracking changes in the combustion chamber.

Chapter 5: Conclusions

The results demonstrate that QWCCR Plasma igniter can be used as a diagnostics tool. Based on in-cylinder pressure there is a corresponding frequency. This frequency is comparable to the resonant frequency found with the network analyzer. Thus this system could be used detect changes in the combustion chamber.

In an advanced version of this system deviations from the operating frequency (to be determined for specific engine and system) could allow for the detection of engine events such as misfires and the completeness of the fuel burn.

With further development and integration of the device, and a control system, into an engine environment, this system could be used as an engine diagnostics tool that is self-adjusting. This self-adjusting system could modify the parameters related to operation of the QWCCR Plasma Igniter in order to operate at the desired operating frequency that is correspondent to the desired outcome in the combustion chamber.

Chapter 6: Recommendations

My recommendations consist of the furthering of this research. This is the first step as proof-of-concept to using this device as a diagnostics tool. A feedback and control system is needed to utilize these diagnostic capabilities. With a control system not only would the device be able to detect things such as misfires, it could make the necessary adjustments in order to correct this problem.

By intelligently controlling the QWCCR with a control system that could adapt it would allow for drastically improved combustion. With the capability to detect incomplete fuel burn the system could change appropriately to correct the issue.

Further, more data needs to be collected with varying fuels and combustion. These different fuels will have different densities and thus affect the resonator in different ways. A lookup table should be compiled to show and utilize the differences between the fuels. The effects will also change depending on the combustion environment, as the pressure and temperature are dependent on the volume of the combustion chamber. This means if the system is to be implemented in a different engine it would be suggested to collect data with different fuels in the new engine.

For these further tests it would also be recommended that new equipment be acquire to improve the testing efficiency and reliability. A completely integrated data collection system would drastically improve the data processing step. Being able to collect the SWR and frequency data on a system that is synced and integrated in to the same system that the pressure and temperature data is collected would be beneficial.

Chapter 7: References

[1] T. J. Bonazza, K. L. VanVoorhies and J. E. Smith, "RF Plasma Ignition System Concept for Lean Burn Internal Combustion Engines," in *SAE Technical Paper 929416*, Warrendale, PA, 1992.

[2] K. L. VanVoorhies, T. J. Bonazza and J. E. Smith, "Analysis of RF Corona Discharge Plasma Ignition," in *SAE Technical Paper 929502*, Warrendale, PA, 1992.

[3] J. E. Smith, R. M. Craven, K. L. VanVoorhies and T. J. Bonzazza, "Radio frequency coaxial cavity resonator as an ignition source and associated method". US Patent US 5,361,737, 08 Nov 1994.

[4] C. A. Stevens, F. A. Pertl, J. L. Hoke, F. R. Schauer and J. E. Smith, "Comparative testing of a novel microwave ignition source, the quarter wave coaxial cavity igniter," *Proceedings of the Institute of Mechnical Engineers, Part D: Journal of Automobile Engineering*, vol. 225, no. 12, pp. 1633-1640, 2011.

[5] "IER," [Online]. Available: http://instituteforenergyresearch.org/topics/encyclopedia/fossil-fuels/. [Accessed 04 Nov 2015].

[6] N. Tesla, "Electrical Igniter for Gas Engines". US Patent US609,250, 16 Aug 1898.

[7] F. R. Simms, "Pulley Toothed Wheel". US Patent US 610,002, 30 Aug 1898.

[8] F. R. Simms and R. Bosch, "Sparking Igniter for Explosion Engines". US Patent US 663,643, 11 Dec 1900.

[9] Y. H. Zweiri, J. F. Whidborne and L. D. Senevirante, "Detailed analytical model of a single-cylinder diseal engine in the crank angle domain," *Institution of Mechanical Engineers,* vol. Vol 215, no. Part D, 2001.

[10] T. J. Bonazza, K. L. VanVoorhies and J. E. Smith, "RF Plasma Ignition System Concept for Lean Burn Internal Combustion Engines," in *SAE Technical Paper 929416*, Warrendale, PA, 1992.

[11] K. L. VanVoorhies, T. J. Bonazza and J. E. Smith, "Analysis of RF Corona Discharge Plasma Ignition," in *SAE Technical Paper 929502*, Warrendale, PA, 1992.

[12] J. E. Smith, R. M. Craven, K. L. VanVoorhies and T. J. Bonazazza, "Radio frequency coaxial cavity resonator as an ignition source and associated method". US Patent 5,361,737,

08 November 1994.

[13] R. Stiles, G. J. Thompson and J. E. Smith, "Investigation of a Radio Frequency Plasma Ignitor for Possible Internal Combustion Engine Use," in *SAE Technical Paper 970071*, Warrendale, PA, 1997.

[14] R. D. Stiles and J. E. Smith, "Modeling the Radio Frequency Coaxial Cavity Plasma Ignitor as an Internal Combustion Engine Ignition System," in *SAE Technical Paper 980168*, Warrendale, PA, 1998.

[15] D. L. Mcintyre, G. J. Thompson and J. E. Smith, "The Coaxial Cavity Resonator as a RF IC Engine Ignition Source," in *SAE Technical Paper 2001-01-0987*, Warrendale, PA, 2001.

[16] A. L. Lowery, F. A. Pertl and J. E. Smith, "Numerical investigation of the quarter wave coaxial cavity resonator quality factor through wire grid modeling in NEC," *22nd Anual Review of Progress in Applied Computational Electromagnetics*, pp. 659-663, 2006.

[17] A. D. Lowery, F. A. Pertl and J. E. Smith, "Experimental investigation of Dielectrics for Use in Quarter Wave Coaxial Resonators," in *SAE Technical Paper 2007-01-0256*, Warrendale, PA, 2007.

[18] "Feasibility of Pulsed Microwave Plasma Ignition for Use in SI-Engines," *ASME 2007 Internal Combustion Engine Division Fall Technical Conference 10.1115/ICEF2007-1776*, pp. 715-719, 2006.

[19] J. E. Smith and F. A. Pertl, "Plasma generating igntion system and associated method". US Patent US 7,721,697 B2, 25 May 2010.

[20] F. A. Pertl and J. E. Smith, "High-Level Modeling of an RF Pulsed Quarter Wave Coaxial Resonator with Potential use as an SI Engine Ignition Source," in *SAE Technical Paper*, Warrendale, PA, 2008.

[21] J. Wilhelm, F. Pertl, P. Willdfire and J. Smith, "Ignition Energy Testing of the Quarter Wave Coaxial Cavity Resonator with Air-Liquefied-Petroleum-Gas Mixtures," in *39th Plasmadynamics and Lasers Conference, American Institute of Aeronautrics and Astronautics*, Seattle, WA, 2008.

[22] F. A. Pertl and J. E. Smith, "Electromagnetic design of a novel microwave internal combustion engine ignition source, the quarter wave coaxial cavity igniter," *Proceedings of the Institution of Mechnical Engineers, Part D: Journal of Automobile Engineering*, vol. 223, no. 11, pp. 1405-1417, 2009.

[23] P. E. Wildfire, A. J. Nawrocki, F. A. Pertl and J. E. Smith, "Investigation of Cold Start Capability of a Briggs and Stratton Engine Using Jet A Fuel and Microwave Plasma Ignition," in *SAE Technical Paper 2009-01-1057*, Warrendale, PA, 2009.

[24] J. E. Smith and F. A. Pertl, "Quarter wave coaxial cavity igniter for combustion engines". US Patent US 8783220 B2, 22 Jul 2014.

[25] J. E. Smith and F. A. Pertl, "Compact electromagnetic plasma ignition device". US Patent US 8887683 B2, 18 Nov 2014.

[26] A. D. Lowery, M. Spencer and J. E. Smith, "Finite Element Analysis of a QWCCR with Dielectric Slugs," in *27th Annual Review of Progress in Applied Computational Electromagnetics, ACES 2011-1067*, 2011.

[27] F. A. Pertl, M. A. Clarke and J. E. Smith, "Design of a compact quarter wave coaxial cavity resonator for plasma ignition applications," *Iternation Journal of Microwave and Wireless Technologies,* vol. 3, no. 04, pp. 485-491, 2011.

[28] M. J. Spencer, A. D. Lowery and J. E. Smtih, "Dual Signal Coaxial Cavity Resonator Plasma Generation". US Patent 20150287574, 8 October 2015.

[29] A. D. Lowery, M. J. Spencer and J. E. Smith, "Method and Apparatus for In-cylinder Combustion Diagnostics". US Patent 61/994,332, 16 May 2014.

[30] P. D. Freen, "System and method for generating and sustaining a corona electric discharge for igniting a combustible gaseous mixture". US Patent 6883507, 26 Apr 2005.

[31] P. D. Freen, "Igniting combustible mixtures". US Patent 8746218 B2, 10 June 2014.

[32] P. D. Freen, "Igniting combustible mixtures". US Patent 20140226252, 14 August 2014.

[33] "Spotidoc," [Online]. Available: http://spotidoc.com/doc/1157631/high-frequency-ignition-system-based-on-corona-discharge. [Accessed 6 November 2015].

[34] T. Giffels, T. Stifel, S. Bohne, G. Ruan and H. Mueller, "Corona ignition device and method for its manufacture". US Patent 8217560 B2, 10 July 2012.

[35] T. Achstaetter, G. Braeuchle, H. Delesky, T. Giffels and F. Heilmann, "HF Ignition Device". US Patent 20110146640 A1, 23 June 2011.

[36] T. Stifel and T. Giffels, "Corona ignition device". US Patent 8550048 B2, 08 October 2013.

[37] T. Stifel, T. Giffels and A. Mueller, "Corona ignition device". US Patent 8767372 B2, 01 July 2014.

[38] M. Allgaier, G. Brauchle, T. Giffels and F. Heilmann, "Igniter for igniting a fuel/air mixture in an internal combustion engine using a corona discharge". US Patent 8860290 B2, 14 October 2014.

[39] T. Giffels, T. Stifel, S. Bohne and H. Muller, "Igniter for igniting a fuel-air-mixture using HF corona discharge and engine fitted with such igniters". US Patent 8857396 B2, 14 October 2014.

[40] Y. Ikeda, A. Nishiyama, Y. Wachi and M. Kaneko, "Research and Development of Microwave Plasma Combustion Engine (Part I: Concept of Plasma Combustion and Plasma Generation Technique," in *SAE Technical Paper 2009-01-1050*, 2009.

[41] Y. Ikeda, A. Nishiyama, H. Katano, M. Kaneko and H. Jeong, "Research and Development of Microwave Plasma Combustion Engine (Part II: Engine Performance of Plasma Combustion Engine)," in *SAE Technical Paper 2009-01-1049*, 2009.

[42] A. Nishiyama and Y. Ikeda, "Improvement of Lean Limit and Fuel Consumption Using Microwave Plasma Ignition Technology," in *SAE technical Paper 2012-01-1139*, 2012.

[43] M. Makita and Y. Ikeda, "Ignition or plasma generation apparatus". US Patent 8226901 B2, 24 July 2012.

[44] M. Makita and Y. Ikeda, "Ignition or plasma generation apparatus". US Patent 20120258016 A1, 11 October 2012.

[45] Y. Ikeda and M. Makita, "United States Patent Application 0140041611 - Plasma Generation Device". US 2014.

[46] J. A. Burrows and J. D. Lykowski, "Multi-event corona discharge ignition assembly and method of control and operation". US Patent 20120145136 A1, 14 June 2012.

[47] J. D. Lykowski, W. J. Walker and J. W. Hoffman, "Igniter system for igniting fuel". US Patent 8434443 B2, 07 May 2013.

[48] A. Permuy and K. Hampton, "Corona tip insulator". US Patent 8464679 B2, 18 June 2013.

[49] A. Permuy and K. Hampton, "Corona ignition with self-tuning power amplifier". US Patent 8578902 B2, 28 May 2013.

[50] J. A. Burrows and J. D. Lykowski, "Corona igniter including ignition coil with improved isolation". US Patent 8638540 B2, 28 January 2014.

[51] J. D. Lykowski, K. Hampton and J. W. W Jr., "Non-thermal plasma ignition arc suppression". US Patent 8729782 B2, 20 May 2014.

[52] J. A. Burrows and J. D. Lykowski, "Electrical arrangement of hybrid ignition device". US Patent 8749945 B2, 10 June 2014.

[53] K. Hampton, J. W. W Jr. and J. D. Lykowski, "Igniter including a corona enhancing electrode tip". US Patent 8776751 B2, 15 July 2014.

[54] J. A. Burrows and J. D. Lykowski, "Corona igniter with magnetic screening". US Patent 8839752 B2, 23 September 2014.

[55] J. A. Burrows, J. D. Lykowski and J. W. Hoffman, "Corona igniter having improved gap control". US Patent 8839753 B2, 23 September 2014.

[56] J. A. Burrows, J. D. Lykowski, A. Permuy and K. Hampton, "Corona igniter having controlled location of corona formation". US Patent 8844490 B2, 30 September 2014.

[57] P. Durham and J. Lykowski, "Corona igniter assembly including corona enhancing insulator geometry". US Patent 8749126 B2, 10 June 2014.

[58] J. A. Burrows and J. D. Lykowski, "Corona igniter including temperature control features". US Patent 9010294 B2, 21 April 2015.

[59] J. A. Burrows and J. D. Lykowski, "Corona igniter having shaped insulator". US Patent 9041273 B2, 26 May 2015.

[60] J. A. Burrows, J. Miller, K. I. Mixell and J. D. Lykowski, "Corona ignition device with improved electrical performance". US Patent 9088136 B2, 21 July 2015.

[61] J. A. Burrows and J. D. Lykowski, "Corona ignition device having asymmetric firing tip". US Patent 9103313 B2, 11 August 2015.

[62] D. K. Cheng, Field and Wave Electromagnetics, Reading, Massachusetts: Addison-Wesley Publishing Co., 1989.

[63] P. Devine, Radar level measurement - The users guide, West Sussex, England: VEGA Controls Ltd., 2000.

[64] A. Lowery, *incylinder_diagnostics_T_P_to_f.m.*

[65] P. Piezotronics, *Model 112B11 Charge Output Pressure Sensor*, March 2013.

Appendix

Appendices A: Matlab Code

A.1: Read_Binary_CFR

```
clear all;

fid=fopen('C:\Users\Trey.Hunsucker\Dropbox\Diagnostics Tests 1-27-16\Data
Logger\Data_PSP-001_012716_15;9;48.bin','r');


RowsPerChannels=1440;


i=1;
EndOfFile=feof(fid);

while (EndOfFile == 0)
      Time(i,1)              = fread(fid, 1,'double');
      EngineSpeed(i,1)       = fread(fid, 1,'double');
      IntakeTemperature(i,1)  = fread(fid, 1,'double');
      ExhaustTemperature(i,1) = fread(fid, 1,'double');
      ChannelNumber(i,1)      = fread(fid, 1,'int');
      Pressure(:,i)          = fread(fid, RowsPerChannels,'int16')/2.0;

       if (min(Pressure(:,i)) < -1000)
          % should have been read as unsigned int16
          fseek(fid, -2*RowsPerChannels, 'cof');
          Pressure(:,i) = fread(fid, RowsPerChannels,'uint16')/2.0;
      end

      i=i+1;
      %Check end of file
      position=ftell(fid);
      testEnd=fread(fid, 1,'double');
      if (feof(fid) == 0)
          fseek(fid,position,'bof');
      else
          EndOfFile = 1;
      end
end

fclose(fid);
```

A.2: Volume Calculation

```
function[CA,V]=CAVolume(Stroke,Bore,CR,VD,Conn)

CA(1)=-180;
V(1)=(VD/(CR-1))+((pi*Bore^2)/4)*(Conn+(Stroke/2)...
      -((Stroke/2)*cos(CA(1)*pi/180)+sqrt((Conn^2)...
      -((Stroke/2)^2)*(sin(CA(1)*pi/180)^2))));
for i=2:1440;
   CA(i,1)=CA(i-1,1)+.25;
   V(i,1)=(VD/(CR-1))+((pi*Bore^2)/4)*(Conn+(Stroke/2)...
      -((Stroke/2)*cos(CA(i,1)*pi/180)+sqrt((Conn^2)...
      -((Stroke/2)^2)*(sin(CA(i,1)*pi/180)^2))));
end
```

A.3: Data Plotting

```
clear;clc;
close all

% Dielectric constant under normal conditions
e_rN = 1.00059;    % Air
CR = 5;            % ICE Compression Ratio

% Normal conditions
T_N = 269.9407581;
P_N = 0.8433084577;

%Import Pressure
P_N_180 = xlsread('DataCLean.xlsx','Baseline','F2:F38'); % Pressure -180
P_N_170 = xlsread('DataCLean.xlsx','Baseline','G2:G38'); % Pressure -170
P_N_160 = xlsread('DataCLean.xlsx','Baseline','H2:H38'); % Pressure -160
P_N_150 = xlsread('DataCLean.xlsx','Baseline','I2:I38'); % Pressure -150
P_N_140 = xlsread('DataCLean.xlsx','Baseline','J2:J38'); % Pressure -140
P_N_130 = xlsread('DataCLean.xlsx','Baseline','K2:K38'); % Pressure -130
P_N_120 = xlsread('DataCLean.xlsx','Baseline','L2:L38'); % Pressure -120
P_N_110 = xlsread('DataCLean.xlsx','Baseline','M2:M38'); % Pressure -110
P_N_100 = xlsread('DataCLean.xlsx','Baseline','N2:N38'); % Pressure -100
P_N_90 = xlsread('DataCLean.xlsx','Baseline','O2:O38'); % Pressure -90
P_N_80 = xlsread('DataCLean.xlsx','Baseline','P2:P38'); % Pressure -80
P_N_70 = xlsread('DataCLean.xlsx','Baseline','Q2:Q38'); % Pressure -70
P_N_60 = xlsread('DataCLean.xlsx','Baseline','R2:R38'); % Pressure -60
P_N_50 = xlsread('DataCLean.xlsx','Baseline','S2:S38'); % Pressure -50
P_N_40  = xlsread('DataCLean.xlsx','Baseline','T2:T38'); % Pressure -40
P_N_30 = xlsread('DataCLean.xlsx','Baseline','U2:U38'); % Pressure -30
P_N_20 = xlsread('DataCLean.xlsx','Baseline','V2:V38'); % Pressure -20
P_N_10 = xlsread('DataCLean.xlsx','Baseline','W2:W38'); % Pressure -10
P_0 = xlsread('DataCLean.xlsx','Baseline','X2:X38'); % Pressure 0
P_10 = xlsread('DataCLean.xlsx','Baseline','Y2:Y38'); % Pressure 10
P_20 = xlsread('DataCLean.xlsx','Baseline','Z2:Z38'); % Pressure 20
P_30 = xlsread('DataCLean.xlsx','Baseline','AA2:AA38'); % Pressure 30
P_40 = xlsread('DataCLean.xlsx','Baseline','AB2:AB38'); % Pressure 40
P_50 = xlsread('DataCLean.xlsx','Baseline','AC2:AC38'); % Pressure 50
P_60 = xlsread('DataCLean.xlsx','Baseline','AD2:AD38'); % Pressure 60
P_70 = xlsread('DataCLean.xlsx','Baseline','AE2:AE38'); % Pressure 70
P_80 = xlsread('DataCLean.xlsx','Baseline','AF2:AF38'); % Pressure 80
P_90 = xlsread('DataCLean.xlsx','Baseline','AG2:AG38'); % Pressure 90
P_100 = xlsread('DataCLean.xlsx','Baseline','AH2:AH38'); % Pressure 100
P_110 = xlsread('DataCLean.xlsx','Baseline','AI2:AI38'); % Pressure 110
P_120 = xlsread('DataCLean.xlsx','Baseline','AJ2:AJ38'); % Pressure 120
P_130 = xlsread('DataCLean.xlsx','Baseline','AK2:AK38'); % Pressure 130
P_140 = xlsread('DataCLean.xlsx','Baseline','AL2:AL38'); % Pressure 140
```

```
P_150 = xlsread('DataCLean.xlsx','Baseline','AM2:AM38'); % Pressure 150
P_160 = xlsread('DataCLean.xlsx','Baseline','AN2:AN38'); % Pressure 160
P_170 = xlsread('DataCLean.xlsx','Baseline','AO2:AO38'); % Pressure 170
P_180 = xlsread('DataCLean.xlsx','Baseline','AP2:AP38'); % Pressure 180
P_BASELINE = xlsread('DataCLean.xlsx','Baseline','AQ2:AQ38'); % Pressure Baseline

%Import Temperature
T_N_180 = xlsread('DataCLean.xlsx','Baseline','F40:F76'); % Temperature -180
T_N_170 = xlsread('DataCLean.xlsx','Baseline','G40:G76'); % Temperature -170
T_N_160 = xlsread('DataCLean.xlsx','Baseline','H40:H76'); % Temperature -160
T_N_150 = xlsread('DataCLean.xlsx','Baseline','I40:I76'); % Temperature -150
T_N_140 = xlsread('DataCLean.xlsx','Baseline','J40:J76'); % Temperature -140
T_N_130 = xlsread('DataCLean.xlsx','Baseline','K40:K76'); % Temperature -130
T_N_120 = xlsread('DataCLean.xlsx','Baseline','L40:L76'); % Temperature -120
T_N_110 = xlsread('DataCLean.xlsx','Baseline','M40:M76'); % Temperature -110
T_N_100 = xlsread('DataCLean.xlsx','Baseline','N40:N76'); % Temperature -100
T_N_90 = xlsread('DataCLean.xlsx','Baseline','O40:O76'); % Temperature -90
T_N_80 = xlsread('DataCLean.xlsx','Baseline','P40:P76'); % Temperature -80
T_N_70 = xlsread('DataCLean.xlsx','Baseline','Q40:Q76'); % Temperature -70
T_N_60 = xlsread('DataCLean.xlsx','Baseline','R40:R76'); % Temperature -60
T_N_50 = xlsread('DataCLean.xlsx','Baseline','S40:S76'); % Temperature -50
T_N_40 = xlsread('DataCLean.xlsx','Baseline','T40:T76'); % Temperature -40
T_N_30 = xlsread('DataCLean.xlsx','Baseline','U40:U76'); % Temperature -30
T_N_20 = xlsread('DataCLean.xlsx','Baseline','V40:V76'); % Temperature -20
T_N_10 = xlsread('DataCLean.xlsx','Baseline','W40:W76'); % Temperature -10
T_0 = xlsread('DataCLean.xlsx','Baseline','X40:X76'); % Temperature 0
T_10 = xlsread('DataCLean.xlsx','Baseline','Y40:Y76'); % Temperature 10
T_20 = xlsread('DataCLean.xlsx','Baseline','Z40:Z76'); % Temperature 20
T_30 = xlsread('DataCLean.xlsx','Baseline','AA40:AA76'); % Temperature 30
T_40 = xlsread('DataCLean.xlsx','Baseline','AB40:AB76'); % Temperature 40
T_50 = xlsread('DataCLean.xlsx','Baseline','AC40:AC76'); % Temperature 50
T_60 = xlsread('DataCLean.xlsx','Baseline','AD40:AD76'); % Temperature 60
T_70 = xlsread('DataCLean.xlsx','Baseline','AE40:AE76'); % Temperature 70
T_80 = xlsread('DataCLean.xlsx','Baseline','AF40:AF76'); % Temperature 80
T_90 = xlsread('DataCLean.xlsx','Baseline','AG40:AG76'); % Temperature 90
T_100 = xlsread('DataCLean.xlsx','Baseline','AH40:AH76'); % Temperature 100
T_110 = xlsread('DataCLean.xlsx','Baseline','AI40:AI76'); % Temperature 110
T_120 = xlsread('DataCLean.xlsx','Baseline','AJ40:AJ76'); % Temperature 120
T_130 = xlsread('DataCLean.xlsx','Baseline','AK40:AK76'); % Temperature 130
T_140 = xlsread('DataCLean.xlsx','Baseline','AL40:AL76'); % Temperature 140
T_150 = xlsread('DataCLean.xlsx','Baseline','AM40:AM76'); % Temperature 150
T_160 = xlsread('DataCLean.xlsx','Baseline','AN40:AN76'); % Temperature 160
T_170 = xlsread('DataCLean.xlsx','Baseline','AO40:AO76'); % Temperature 170
T_180 = xlsread('DataCLean.xlsx','Baseline','AP40:AP76'); % Temperature 180
T_BASELINE = xlsread('DataCLean.xlsx','Baseline','AQ40:AQ76'); % Temperature Baseline
```

```
%Import Frequency
F_N_180 = xlsread('DataCLean.xlsx','Baseline','F116:F152'); % Frequency -180
F_N_170 = xlsread('DataCLean.xlsx','Baseline','G116:G152'); % Frequency -170
F_N_160 = xlsread('DataCLean.xlsx','Baseline','H116:H152'); % Frequency -160
F_N_150 = xlsread('DataCLean.xlsx','Baseline','I116:I152'); % Frequency -150
F_N_140 = xlsread('DataCLean.xlsx','Baseline','J116:J152'); % Frequency -140
F_N_130 = xlsread('DataCLean.xlsx','Baseline','K116:K152'); % Frequency -130
F_N_120 = xlsread('DataCLean.xlsx','Baseline','L116:L152'); % Frequency -120
F_N_110 = xlsread('DataCLean.xlsx','Baseline','M116:M152'); % Frequency -110
F_N_100 = xlsread('DataCLean.xlsx','Baseline','N116:N152'); % Frequency -100
F_N_90 = xlsread('DataCLean.xlsx','Baseline','O116:O152'); % Frequency -90
F_N_80 = xlsread('DataCLean.xlsx','Baseline','P116:P152'); % Frequency -80
F_N_70 = xlsread('DataCLean.xlsx','Baseline','Q116:Q152'); % Frequency -70
F_N_60 = xlsread('DataCLean.xlsx','Baseline','R116:R152'); % Frequency -60
F_N_50 = xlsread('DataCLean.xlsx','Baseline','S116:S152'); % Frequency -50
F_N_40 = xlsread('DataCLean.xlsx','Baseline','T116:T152'); % Frequency -40
F_N_30 = xlsread('DataCLean.xlsx','Baseline','U116:U152'); % Frequency -30
F_N_20 = xlsread('DataCLean.xlsx','Baseline','V116:V152'); % Frequency -20
F_N_10 = xlsread('DataCLean.xlsx','Baseline','W116:W152'); % Frequency -10
F_0 = xlsread('DataCLean.xlsx','Baseline','X116:X152'); % Frequency 0
F_10 = xlsread('DataCLean.xlsx','Baseline','Y116:Y152'); % Frequency 10
F_20 = xlsread('DataCLean.xlsx','Baseline','Z116:Z152'); % Frequency 20
F_30 = xlsread('DataCLean.xlsx','Baseline','AA116:AA152'); % Frequency 30
F_40 = xlsread('DataCLean.xlsx','Baseline','AB116:AB152'); % Frequency 40
F_50 = xlsread('DataCLean.xlsx','Baseline','AC116:AC152'); % Frequency 50
F_60 = xlsread('DataCLean.xlsx','Baseline','AD116:AD152'); % Frequency 60
F_70 = xlsread('DataCLean.xlsx','Baseline','AE116:AE152'); % Frequency 70
F_80 = xlsread('DataCLean.xlsx','Baseline','AF116:AF152'); % Frequency 80
F_90 = xlsread('DataCLean.xlsx','Baseline','AG116:AG152'); % Frequency 90
F_100 = xlsread('DataCLean.xlsx','Baseline','AH116:AH152'); % Frequency 100
F_110 = xlsread('DataCLean.xlsx','Baseline','AI116:AI152'); % Frequency 110
F_120 = xlsread('DataCLean.xlsx','Baseline','AJ116:AJ152'); % Frequency 120
F_130 = xlsread('DataCLean.xlsx','Baseline','AK116:AK152'); % Frequency 130
F_140 = xlsread('DataCLean.xlsx','Baseline','AL116:AL152'); % Frequency 140
F_150 = xlsread('DataCLean.xlsx','Baseline','AM116:AM152'); % Frequency 150
F_160 = xlsread('DataCLean.xlsx','Baseline','AN116:AN152'); % Frequency 160
F_170 = xlsread('DataCLean.xlsx','Baseline','AO116:AO152'); % Frequency 170
F_180 = xlsread('DataCLean.xlsx','Baseline','AP116:AP152'); % Frequency 180
F_BASELINE = xlsread('DataCLean.xlsx','Baseline','AQ116:AQ152'); % Frequency Baseline
F_E = xlsread('DataCLean.xlsx','Baseline','E2:E38'); % Frequency Experimental

%Import Density
D_N_180 = xlsread('DataCLean.xlsx','Baseline','F193:F229'); % Density -180
D_N_170 = xlsread('DataCLean.xlsx','Baseline','G193:G229'); % Density -170
D_N_160 = xlsread('DataCLean.xlsx','Baseline','H193:H229'); % Density -160
D_N_150 = xlsread('DataCLean.xlsx','Baseline','I193:I229'); % Density -150
```

```
D_N_140 = xlsread('DataCLean.xlsx','Baseline','J193:J229'); % Density -140
D_N_130 = xlsread('DataCLean.xlsx','Baseline','K193:K229'); % Density -130
D_N_120 = xlsread('DataCLean.xlsx','Baseline','L193:L229'); % Density -120
D_N_110 = xlsread('DataCLean.xlsx','Baseline','M193:M229'); % Density -110
D_N_100 = xlsread('DataCLean.xlsx','Baseline','N193:N229'); % Density -100
D_N_90 = xlsread('DataCLean.xlsx','Baseline','O193:O229'); % Density -90
D_N_80 = xlsread('DataCLean.xlsx','Baseline','P193:P229'); % Density -80
D_N_70 = xlsread('DataCLean.xlsx','Baseline','Q193:Q229'); % Density -70
D_N_60 = xlsread('DataCLean.xlsx','Baseline','R193:R229'); % Density -60
D_N_50 = xlsread('DataCLean.xlsx','Baseline','S193:S229'); % Density -50
D_N_40 = xlsread('DataCLean.xlsx','Baseline','T193:T229'); % Density -40
D_N_30 = xlsread('DataCLean.xlsx','Baseline','U193:U229'); % Density -30
D_N_20 = xlsread('DataCLean.xlsx','Baseline','V193:V229'); % Density -20
D_N_10 = xlsread('DataCLean.xlsx','Baseline','W193:W229'); % Density -10
D_0 = xlsread('DataCLean.xlsx','Baseline','X193:X229'); % Density 0
D_10 = xlsread('DataCLean.xlsx','Baseline','Y193:Y229'); % Density 10
D_20 = xlsread('DataCLean.xlsx','Baseline','Z193:Z229'); % Density 20
D_30 = xlsread('DataCLean.xlsx','Baseline','AA193:AA229'); % Density 30
D_40 = xlsread('DataCLean.xlsx','Baseline','AB193:AB229'); % Density 40
D_50 = xlsread('DataCLean.xlsx','Baseline','AC193:AC229'); % Density 50
D_60 = xlsread('DataCLean.xlsx','Baseline','AD193:AD229'); % Density 60
D_70 = xlsread('DataCLean.xlsx','Baseline','AE193:AE229'); % Density 70
D_80 = xlsread('DataCLean.xlsx','Baseline','AF193:AF229'); % Density 80
D_90 = xlsread('DataCLean.xlsx','Baseline','AG193:AG229'); % Density 90
D_100 = xlsread('DataCLean.xlsx','Baseline','AH193:AH229'); % Density 100
D_110 = xlsread('DataCLean.xlsx','Baseline','AI193:AI229'); % Density 110
D_120 = xlsread('DataCLean.xlsx','Baseline','AJ193:AJ229'); % Density 120
D_130 = xlsread('DataCLean.xlsx','Baseline','AK193:AK229'); % Density 130
D_140 = xlsread('DataCLean.xlsx','Baseline','AL193:AL229'); % Density 140
D_150 = xlsread('DataCLean.xlsx','Baseline','AM193:AM229'); % Density 150
D_160 = xlsread('DataCLean.xlsx','Baseline','AN193:AN229'); % Density 160
D_170 = xlsread('DataCLean.xlsx','Baseline','AO193:AO229'); % Density 170
D_180 = xlsread('DataCLean.xlsx','Baseline','AP193:AP229'); % Density 180
D_BASELINE = xlsread('DataCLean.xlsx','Baseline','AQ193:AQ229'); % Density Baseline
D_E = xlsread('DataCLean.xlsx','Baseline','H231:H267'); % Density from Frequency

CA = xlsread('DataCLean.xlsx','Baseline','A2:A38');


%Temperature and pressure ranges
Num_points = 37;
for index = 1:length(CR)
   F(index,:) = linspace(300,500,Num_points);
   P(index,:) = linspace(1,CR(index).^1.4,Num_points);
```

```
% Change in permittivity
e_r = 1 + (e_rN - 1)*((T_N.*P(index,:))./(T(index,:).*P_N));

% Change in frequency
f = 1;
f_e_r(index,:) = f./sqrt(e_r);

end

%Baseline pressure
figure (1)
plot(CA(:,1),P_N_180(:,1),...
    CA(:,1),P_N_170(:,1),...
    CA(:,1),P_N_160(:,1),...
    CA(:,1),P_N_150(:,1),...
    CA(:,1),P_N_140(:,1),...
    CA(:,1),P_N_130(:,1),...
    CA(:,1),P_N_120(:,1),...
    CA(:,1),P_N_110(:,1),...
    CA(:,1),P_N_100(:,1),...
    CA(:,1),P_N_90(:,1),...
    CA(:,1),P_N_80(:,1),...
    CA(:,1),P_N_70(:,1),...
    CA(:,1),P_N_60(:,1),...
    CA(:,1),P_N_50(:,1),...
    CA(:,1),P_N_40(:,1),...
    CA(:,1),P_N_30(:,1),...
    CA(:,1),P_N_20(:,1),...
    CA(:,1),P_N_10(:,1),...
    CA(:,1),P_0(:,1),...
    CA(:,1),P_10(:,1),...
    CA(:,1),P_20(:,1),...
    CA(:,1),P_30(:,1),...
    CA(:,1),P_40(:,1),...
    CA(:,1),P_50(:,1),...
    CA(:,1),P_60(:,1),...
    CA(:,1),P_70(:,1),...
    CA(:,1),P_80(:,1),...
    CA(:,1),P_90(:,1),...
    CA(:,1),P_100(:,1),...
    CA(:,1),P_110(:,1),...
    CA(:,1),P_120(:,1),...
    CA(:,1),P_130(:,1),...
    CA(:,1),P_140(:,1),...
    CA(:,1),P_150(:,1),...
    CA(:,1),P_160(:,1),...
```

```
    CA(:,1),P_170(:,1),...
    CA(:,1),P_180(:,1))
hold on
   plot(CA(:,1),P_BASELINE(:,1),'k','LineWidth',4)
x1=[-156.,-156.5];
x2=[130.5,130.5];
y=[0,1000000];
plot(x1,y,'--k',x2,y,'--k','LineWidth',1)
title('Plot of Baseline Pressure (Pa) vs Change in Crank Angle')
xlabel('Crank Angle (degree)')
ylabel('Pressure (Pa)')
xlim([min(min(CA)) max(max(CA))])
ylim([min(min(P_BASELINE)) max(max(P_BASELINE)*1.05)])
hold off

%Baseline temperature
figure (2)
plot(CA(:,1),T_N_180(:,1),...
    CA(:,1),T_N_170(:,1),...
    CA(:,1),T_N_160(:,1),...
    CA(:,1),T_N_150(:,1),...
    CA(:,1),T_N_140(:,1),...
    CA(:,1),T_N_130(:,1),...
    CA(:,1),T_N_120(:,1),...
    CA(:,1),T_N_110(:,1),...
    CA(:,1),T_N_100(:,1),...
    CA(:,1),T_N_90(:,1),...
    CA(:,1),T_N_80(:,1),...
    CA(:,1),T_N_70(:,1),...
    CA(:,1),T_N_60(:,1),...
    CA(:,1),T_N_50(:,1),...
    CA(:,1),T_N_40(:,1),...
    CA(:,1),T_N_30(:,1),...
    CA(:,1),T_N_20(:,1),...
    CA(:,1),T_N_10(:,1),...
    CA(:,1),T_0(:,1),...
    CA(:,1),T_10(:,1),...
    CA(:,1),T_20(:,1),...
    CA(:,1),T_30(:,1),...
    CA(:,1),T_40(:,1),...
    CA(:,1),T_50(:,1),...
    CA(:,1),T_60(:,1),...
    CA(:,1),T_70(:,1),...
    CA(:,1),T_80(:,1),...
    CA(:,1),T_90(:,1),...
    CA(:,1),T_100(:,1),...
```

```
    CA(:,1),T_110(:,1),...
    CA(:,1),T_120(:,1),...
    CA(:,1),T_130(:,1),...
    CA(:,1),T_140(:,1),...
    CA(:,1),T_150(:,1),...
    CA(:,1),T_160(:,1),...
    CA(:,1),T_170(:,1),...
    CA(:,1),T_180(:,1))
hold on
   plot(CA(:,1),T_BASELINE(:,1),'k','LineWidth',4)
x1=[-156.,-156.5];
x2=[130.5,130.5];
y=[0,1200];
plot(x1,y,'--k',x2,y,'--k','LineWidth',1)
title('Plot of Baseline Temperature (K) vs Change in Crank Angle')
xlabel('Crank Angle (degree)')
ylabel('Temperature (K)')
xlim([min(min(CA)) max(max(CA))])
ylim([min(min(T_BASELINE)) max(700)])
hold off

%Baseline frequency
figure (3)
plot(CA(:,1),F_E(:,1),...
    CA(:,1),F_N_180(:,1),...
    CA(:,1),F_N_170(:,1),...
    CA(:,1),F_N_160(:,1),...
    CA(:,1),F_N_150(:,1),...
    CA(:,1),F_N_140(:,1),...
    CA(:,1),F_N_130(:,1),...
    CA(:,1),F_N_120(:,1),...
    CA(:,1),F_N_110(:,1),...
    CA(:,1),F_N_100(:,1),...
    CA(:,1),F_N_90(:,1),...
    CA(:,1),F_N_80(:,1),...
    CA(:,1),F_N_70(:,1),...
    CA(:,1),F_N_60(:,1),...
    CA(:,1),F_N_50(:,1),...
    CA(:,1),F_N_40(:,1),...
    CA(:,1),F_N_30(:,1),...
    CA(:,1),F_N_20(:,1),...
    CA(:,1),F_N_10(:,1),...
    CA(:,1),F_0(:,1),...
    CA(:,1),F_10(:,1),...
    CA(:,1),F_20(:,1),...
    CA(:,1),F_30(:,1),...
```

```
    CA(:,1),F_40(:,1),...
    CA(:,1),F_50(:,1),...
    CA(:,1),F_60(:,1),...
    CA(:,1),F_70(:,1),...
    CA(:,1),F_80(:,1),...
    CA(:,1),F_90(:,1),...
    CA(:,1),F_100(:,1),...
    CA(:,1),F_110(:,1),...
    CA(:,1),F_120(:,1),...
    CA(:,1),F_130(:,1),...
    CA(:,1),F_140(:,1),...
    CA(:,1),F_150(:,1),...
    CA(:,1),F_160(:,1),...
    CA(:,1),F_170(:,1),...
    CA(:,1),F_180(:,1))
hold on
   plot(CA(:,1),F_BASELINE(:,1),'k','LineWidth',4)
x1=[-156.,-156.5];
x2=[130.5,130.5];
y=[0,10000000000000];
plot(x1,y,'--k',x2,y,'--k','LineWidth',1)
title('Plot of Baseline Frequency (GHz) vs Change in Crank Angle')
xlabel('Crank Angle (degree)')
ylabel('Frequency (GHz)')
xlim([min(min(CA)) max(max(CA))])
ylim([min(min(F_BASELINE)*.999) max(max(F_E)*1.005)])
hold off

%Density
figure (4)
plot(CA(:,1),D_N_180(:,1),...
    CA(:,1),D_N_170(:,1),...
    CA(:,1),D_N_160(:,1),...
    CA(:,1),D_N_150(:,1),...
    CA(:,1),D_N_140(:,1),...
    CA(:,1),D_N_130(:,1),...
    CA(:,1),D_N_120(:,1),...
    CA(:,1),D_N_110(:,1),...
    CA(:,1),D_N_100(:,1),...
    CA(:,1),D_N_90(:,1),...
    CA(:,1),D_N_80(:,1),...
    CA(:,1),D_N_70(:,1),...
    CA(:,1),D_N_60(:,1),...
    CA(:,1),D_N_50(:,1),...
    CA(:,1),D_N_40(:,1),...
    CA(:,1),D_N_30(:,1),...
```

```
    CA(:,1),D_N_20(:,1),...
    CA(:,1),D_N_10(:,1),...
    CA(:,1),D_0(:,1),...
    CA(:,1),D_10(:,1),...
    CA(:,1),D_20(:,1),...
    CA(:,1),D_30(:,1),...
    CA(:,1),D_40(:,1),...
    CA(:,1),D_50(:,1),...
    CA(:,1),D_60(:,1),...
    CA(:,1),D_70(:,1),...
    CA(:,1),D_80(:,1),...
    CA(:,1),D_90(:,1),...
    CA(:,1),D_100(:,1),...
    CA(:,1),D_110(:,1),...
    CA(:,1),D_120(:,1),...
    CA(:,1),D_130(:,1),...
    CA(:,1),D_140(:,1),...
    CA(:,1),D_150(:,1),...
    CA(:,1),D_160(:,1),...
    CA(:,1),D_170(:,1),...
    CA(:,1),D_180(:,1))
hold on
   plot(CA(:,1),D_BASELINE(:,1),'k','LineWidth',4)
   plot(CA(:,1),D_E(:,1),'b','Linewidth',2)
x1=[-156.,-156.5];
x2=[130.5,130.5];
y=[0,1000];
plot(x1,y,'--k',x2,y,'--k','LineWidth',1)
title('Plot of Baseline Density (kg/m^3) vs Change in Crank Angle')
xlabel('Crank Angle (degree)')
ylabel('Density (kg/m^3)')
xlim([min(min(CA)) max(max(CA))])
ylim([min(min(0)) max(max(7.5))])
hold off



%Surface plot for CR(1);
[T, P] = meshgrid(T(1,:),P(1,:));
f_e_r = f./sqrt(1 + (e_rN - 1)*((T_N.*P)./(T.*P_N)));

figure(5)
mesh(P_BASELINE,CA,F_BASELINE)
xlabel('Pressure (Pa)')
ylabel('Crank Angle')
```

```
zlabel('Frequency (GHz)')
xlim([min(min(P_BASELINE)) max(max(P_BASELINE))])
ylim([min(min(CA)) max(max(CA))])
zlim([min(min(F_BASELINE)) max(max(F_BASELINE))])
view([-120 120])

figure(6)
mesh(P_BASELINE,CA,F_E)
xlabel('Pressure (Pa)')
ylabel('Crank Angle')
zlabel('Frequency (GHz)')
xlim([min(min(P_BASELINE)) max(max(P_BASELINE))])
ylim([min(min(CA)) max(max(CA))])
zlim([min(min(F_E)) max(max(F_E))])
view([-120 120])
```

Appendices B: Raw Data

B.1: Volume of Cylinder by Crank Angle

	Volume (m^3)
-180	0.000764745
-170	0.000761128
-160	0.000750298
-150	0.000732328
-140	0.000707364
-130	0.000675667
-120	0.000637659
-110	0.000593974
-100	0.000545509
-90	0.000493451
-80	0.000439281
-70	0.000384745
-60	0.000331786
-50	0.000282445
-40	0.00023874
-30	0.000202541
-20	0.000175446
-10	0.000158677
0	0.000153
10	0.000158677
20	0.000175446
30	0.000202541
40	0.00023874
50	0.000282445
60	0.000331786
70	0.000384745
80	0.000439281
90	0.000493451
100	0.000545509
110	0.000593974
120	0.000637659
130	0.000675667
140	0.000707364
150	0.000732328
160	0.000750298
170	0.000761128
180	0.000764745

B.2: Pressure Data (Pa)

	P -180	P -170	P -160	P -150	P -140	P -130	P -120	P -110	P -100	P -90	P -80	P -70	P -60
-180	84331	75000	79500	88000	79500	76500	63500	90000	82000	63500	81000	75000	53000
-170	89786	76000	65500	92500	92500	97000	102500	90000	132500	102000	83000	76000	110500
-160	87159	84500	56000	91000	96500	100500	99500	77000	76000	127000	101500	84500	88500
-150	87261	58000	87000	46000	77500	107500	78000	81000	56500	51000	115000	58000	105000
-140	91836	82000	57500	57500	69000	66000	97500	67500	115500	101500	100000	82000	119000
-130	91072	115500	90000	72500	109500	121500	74000	81000	86500	103500	102000	115500	81000
-120	108863	106500	94000	97500	81000	92500	100000	91000	96500	75000	93000	106500	82000
-110	114719	56000	83500	110000	89000	82500	99500	115000	108500	113000	96500	56000	114500
-100	117796	98500	101000	105000	128500	130500	135500	105000	95500	110000	118000	98500	117000
-90	157209	133500	124500	105500	134500	137000	122000	152500	134500	132000	125000	133500	94500
-80	149741	152000	127000	161500	121500	151500	133000	155000	133500	119500	164000	152000	123000
-70	222206	155500	147500	187500	172000	144000	172000	157500	157000	180000	183500	155500	154500
-60	247953	199500	201000	197500	230000	192000	214500	200000	185000	210500	220000	199500	180000
-50	257216	246000	205500	240000	263500	223500	195500	261500	281500	218500	226000	246000	246000
-40	433644	264500	323000	278000	309000	315500	295000	337500	284500	318500	283000	264500	318000
-30	483744	386500	353500	395500	348000	349000	388500	400500	373500	359000	381500	386500	370000
-20	502709	464000	490000	484000	475500	467500	481500	465000	498500	503000	464000	464000	536000
-10	759659	609500	584500	606500	566500	598500	623000	616500	592000	574500	611000	609500	588500
0	795806	809500	790000	781000	795000	807000	776000	789000	765000	796000	800500	809500	820500
10	751585	767500	767500	777000	801500	808000	800000	785500	737000	768500	788500	767500	761000
20	698348	774000	813500	817000	768000	787500	785500	790000	756500	765000	759000	774000	802500
30	689361	719000	708000	734000	716500	710500	698000	739000	738000	714500	690000	719000	703500
40	411545	593000	582500	633000	614500	584000	572000	589500	575500	602500	573000	593000	585000
50	378117	484500	479000	470000	474000	478500	431000	467500	468000	461000	455500	484500	470500
60	296040	338500	387500	349500	377000	358500	385000	361000	378500	385000	352500	338500	364500

70	202100	219500	213000	260500	204000	228000	185000	191000	176500	218000	260500	219500	172000
80	170726	134000	149500	146500	175000	157500	165000	178500	189500	163500	180500	134000	201500
90	139107	163000	124000	125500	117500	153000	114500	112000	125000	147500	131000	163000	127000
100	129888	168000	143000	144500	138000	162000	159500	126000	153500	125000	155500	168000	138000
110	126565	165000	157500	134000	105000	163000	117500	115500	137000	129500	112000	165000	152000
120	93465	132000	93500	102000	102500	118500	98000	116500	111500	116500	99000	132000	115500
130	88405	138000	111500	121000	81000	106000	105000	77500	96000	76000	116000	138000	124500
140	90973	106000	78500	95000	69500	109500	99000	121000	74000	111000	97000	106000	112000
150	75910	73000	65000	64500	64500	63000	108000	76000	54000	76000	92500	73000	59000
160	79806	93500	58500	91000	93000	65000	78000	86000	69500	80000	96500	93500	64500
170	77923	109500	83000	75000	49500	102000	96500	84000	69500	91500	88500	109500	67500
180	82303	71500	105500	71500	98500	88000	101000	77500	77000	80000	106000	71500	80500

P -50	P -40	P -30	P -20	P -10	P 0	P 10	P 20	P 30	P 40	P 50	P 60	P 70	P 80
101500	72500	57000	77500	63500	67000	74500	102500	63500	107000	79500	123500	83500	106000
91500	95500	84500	74500	88000	53500	83500	81500	104500	113000	92500	90000	116000	122000
84500	89000	97500	90000	58500	81000	114000	91000	87500	62000	96500	60500	78000	106000
121000	82000	80000	67000	91000	106500	129000	106000	88000	99000	77500	63500	115500	60500
109500	67000	56500	94000	75500	86500	67500	127500	129000	99000	69000	81500	89000	103000
110000	72500	91000	80000	108000	71000	87000	71000	97000	65000	109500	116000	80000	64500
74500	74000	125500	112000	101000	100500	118000	101000	87500	112500	81000	132500	85000	106000
69500	145000	93000	109000	103500	128500	109500	74000	98000	137000	89000	108500	91000	88500
139000	95000	122500	114500	80000	113000	163500	79000	118000	142500	128500	92000	124500	101500
92500	123500	144500	113000	115500	136000	139000	120000	136500	124000	134500	127500	119500	98000
142000	166000	155500	150500	159000	108500	163500	189000	112500	146000	121500	139500	126000	145000
170500	160500	215000	170500	160500	170500	179000	176500	171500	192000	172000	148000	192000	175500
182500	198000	174000	228000	212500	202000	187000	206000	180500	218000	230000	215500	229000	192000

215000	236000	265000	262000	212500	249500	252500	225000	245000	259500	263500	245500	235000	218000
325500	278000	325000	298000	299500	291500	302000	268000	328500	303500	309000	311500	318500	303000
366000	372500	410500	358500	398000	373000	352000	383000	394000	377500	348000	418000	397500	351000
454000	439500	485500	477000	448500	519500	486500	448000	484000	482500	475500	485500	481500	464500
590000	595500	583000	607500	621000	606000	578000	608500	609500	565000	566500	580500	620500	586500
805000	781500	791500	809500	811500	810500	776000	784500	820000	792500	795000	804000	800000	751500
810000	765000	753500	792000	757500	765000	766500	828000	783500	742500	801500	813500	802000	795500
785500	797500	803500	825500	774000	789000	778500	791000	786000	801500	768000	779000	817000	771000
693500	729000	658000	712500	756000	701000	727500	732000	678000	724000	716500	696500	739500	688500
612000	623500	590500	602000	583500	604500	640000	594000	605000	602000	614500	609500	599000	616000
467500	480000	488000	470500	504000	462000	483000	441500	472500	465500	474000	480000	465500	469500
348000	387500	360500	404500	387500	379000	355000	369000	407500	379500	377000	401500	387500	391500
207500	229000	205000	205000	189500	222500	243000	212000	206500	201500	204000	205500	205500	212500
174000	187500	118000	163000	165500	213000	173000	143000	182500	135500	175000	150000	157000	168000
138500	109000	134500	143000	123500	96500	124500	132000	149500	142000	117500	164000	149000	131000
174000	182500	133000	146000	153500	148500	132000	125500	153500	126500	138000	124000	134500	179000
126500	187500	127000	155500	124000	125000	84500	147000	135000	140500	105000	87000	104000	97000
95000	147000	123500	125500	136500	101000	141000	150000	96500	142000	102500	113500	132500	122500
94000	134000	92000	118500	74500	102500	113500	95500	72500	99000	81000	106000	71500	78500
89000	72500	66000	95500	83000	93000	74500	84500	111000	105500	69500	92000	107000	54500
74000	114000	85500	49500	64500	84000	95500	77500	86500	94500	64500	100000	102500	76000
61500	70000	72000	91500	110500	129500	68500	89500	79500	87500	93000	105500	81000	80500
55500	51000	79000	72500	67000	53500	87500	82000	79500	72500	49500	91500	68500	46000
55500	92500	65500	114500	82500	61000	77500	74000	91500	68000	98500	103500	55500	87000

P 90	P 100	P 110	P 120	P 130	P 140	P 150	P 160	P 170	P 180	Baseline Average
67000	66500	63500	106000	67000	66500	120500	63500	89500	79500	84280

53500	81500	102500	122000	53500	81500	111500	104500	128500	92500	90095
81000	81000	99500	106000	81000	81000	103000	87500	87000	96500	87234
106500	73000	78000	60500	106500	73000	60500	88000	81000	77500	85395
86500	119000	97500	103000	86500	119000	110000	129000	76000	69000	87310
71000	77000	74000	64500	71000	77000	106000	97000	64000	109500	90249
100500	99000	100000	106000	100500	99000	124000	87500	77500	81000	95860
128500	96500	99500	88500	128500	96500	119500	98000	121500	89000	113875
113000	112500	135500	101500	113000	112500	105500	118000	114500	128500	113875
136000	112000	122000	98000	136000	112000	93500	136500	150000	134500	125265
108500	134000	133000	145000	108500	134000	123500	112500	123000	121500	142990
170500	148000	172000	175500	170500	148000	157500	171500	158000	172000	166560
202000	195500	214500	192000	202000	195500	214000	180500	161500	230000	201545
249500	228000	195500	218000	249500	228000	225000	245000	223500	263500	242525
291500	272000	295000	303000	291500	272000	318000	328500	331500	309000	301145
373000	355000	388500	351000	373000	355000	397500	394000	386500	348000	374715
519500	481500	481500	464500	519500	481500	516000	484000	516500	475500	475655
606000	599500	623000	586500	606000	599500	615500	609500	608500	566500	591375
810500	784000	776000	751500	810500	784000	794500	820000	804000	795000	796010
765000	767000	800000	795500	765000	767000	778000	783500	765500	801500	782495
789000	784500	785500	771000	789000	784500	822500	786000	813500	768000	782495
701000	716000	698000	688500	701000	716000	731500	678000	703000	716500	718150
604500	558000	572000	616000	604500	558000	594000	605000	566500	614500	599945
462000	451000	431000	469500	462000	451000	481000	472500	494500	474000	477615
379000	341500	385000	391500	379000	341500	373500	407500	372500	377000	371940
222500	181000	185000	212500	222500	181000	224000	206500	186500	204000	203325
213000	194000	165000	168000	213000	194000	188000	182500	175000	175000	170595
96500	126000	114500	131000	96500	126000	126000	149500	99000	117500	135890
148500	161000	159500	179000	148500	161000	151000	153500	165500	138000	153940

125000	123000	117500	97000	125000	123000	162500	135000	128500	105000	129005
101000	80500	98000	122500	101000	80500	112000	96500	148000	102500	114665
102500	78000	105000	78500	102500	78000	101000	72500	89500	81000	99605
93000	82000	99000	54500	93000	82000	113000	111000	100000	69500	92350
84000	108500	108000	76000	84000	108500	98500	86500	76000	64500	92350
129500	113500	78000	80500	129500	113500	65000	79500	100000	93000	81205
53500	49000	96500	46000	53500	49000	87500	79500	81500	49500	75515
61000	59000	101000	87000	61000	59000	51500	91500	62500	98500	82020

B.3: Temperature Data (K)

	-180	-170	-160	-150	-140	-130	-120	-110	-100	-90	-80	-70	-60
-180	289	289	289	289	289	289	289	289	289	289	289	289	289
-170	284	253	268	296	268	258	214	303	276	214	273	253	178
-160	301	255	219	310	310	325	343	302	444	342	278	255	370
-150	288	279	185	301	319	332	329	254	251	419	335	279	292
-140	281	187	280	148	250	347	251	261	182	164	371	187	339
-130	286	255	179	179	215	206	304	210	360	316	311	255	371
-120	271	344	268	216	326	361	220	241	257	308	303	344	241
-110	306	299	264	274	227	260	281	255	271	211	261	299	230
-100	300	146	218	288	233	216	260	301	284	295	252	146	299
-90	283	237	243	252	309	313	325	252	229	264	283	237	281
-80	342	290	270	229	292	298	265	331	292	287	272	290	205
-70	290	294	246	312	235	293	257	300	258	231	317	294	238
-60	376	263	250	318	291	244	291	267	266	305	311	263	262
-50	362	291	294	288	336	280	313	292	270	307	321	291	263
-40	320	306	256	298	328	278	243	325	350	272	281	306	306
-30	456	278	339	292	325	332	310	355	299	335	297	278	334
-20	431	345	315	353	310	311	346	357	333	320	340	345	330
-10	388	358	378	374	367	361	372	359	385	389	358	358	414
0	531	426	408	424	396	418	435	431	414	401	427	426	411
10	536	545	532	526	535	544	523	531	515	536	539	545	553
20	525	536	536	543	560	564	559	549	515	537	551	536	532
30	539	598	628	631	593	608	607	610	584	591	586	598	620
40	615	641	631	654	639	634	622	659	658	637	615	641	627
50	433	623	612	665	646	614	601	620	605	633	602	623	615
60	470	602	596	584	589	595	536	581	582	573	566	602	585

70	432	494	566	510	551	524	562	527	553	562	515	494	532
80	342	372	361	441	346	386	313	324	299	369	441	372	291
90	330	259	289	283	338	305	319	345	366	316	349	259	390
100	302	354	269	273	255	332	249	243	272	320	285	354	276
110	312	403	343	347	331	389	383	303	369	300	373	403	331
120	331	431	412	350	275	426	307	302	358	339	293	431	397
130	262	371	262	286	288	333	275	327	313	327	278	371	324
140	263	410	332	360	241	315	312	231	286	226	345	410	370
150	283	330	244	296	216	341	308	377	230	346	302	330	349
160	245	235	210	208	208	203	348	245	174	245	298	235	190
170	264	309	193	301	307	215	258	284	230	264	319	309	213
180	261	367	278	251	166	342	323	281	233	307	297	367	226

-50	-40	-30	-20	-10	0	10	20	30	40	50	60	70	80
289	289	289	289	289	289	289	289	289	289	289	289	289	289
342	244	192	261	214	226	251	345	214	360	268	416	281	357
307	320	283	250	295	179	280	273	350	379	310	302	389	409
279	294	322	297	193	268	377	301	289	205	319	200	258	350
390	264	258	216	293	343	416	342	284	319	250	205	372	195
341	209	176	293	235	269	210	397	402	308	215	254	277	321
327	216	271	238	321	211	259	211	289	193	326	345	238	192
209	208	352	314	284	282	331	284	246	316	227	372	239	298
182	379	243	285	271	336	286	194	256	358	233	284	238	231
334	228	294	275	192	271	393	190	283	342	309	221	299	244
201	268	314	245	251	295	302	261	297	269	292	277	260	213
275	321	301	291	307	210	316	366	218	282	235	270	244	280
289	272	364	289	272	289	303	299	290	325	291	251	325	297

267	289	254	333	310	295	273	301	264	318	336	315	334	280
267	293	330	326	264	310	314	280	305	323	328	305	292	271
342	292	342	313	315	306	317	282	345	319	325	327	335	318
326	332	366	320	355	333	314	342	351	337	310	373	354	313
351	339	375	368	346	401	376	346	374	373	367	375	372	359
412	416	407	424	434	423	404	425	426	395	396	406	433	410
542	526	533	545	547	546	523	528	552	534	535	542	539	506
566	534	526	553	529	534	535	578	547	519	560	568	560	556
607	616	621	638	598	609	601	611	607	619	593	602	631	596
618	650	587	635	674	625	649	653	605	646	639	621	659	614
643	655	621	633	613	635	673	624	636	633	646	641	630	647
581	597	607	585	627	574	601	549	588	579	589	597	579	584
508	566	527	591	566	554	519	539	595	554	551	586	566	572
351	388	347	347	321	377	412	359	350	341	346	348	348	360
336	363	228	315	320	412	335	277	353	262	338	290	304	325
301	237	292	311	268	210	270	287	325	308	255	356	324	285
418	438	319	351	369	357	317	301	369	304	331	298	323	430
331	490	332	407	324	327	221	384	353	367	275	227	272	254
267	413	347	352	383	284	396	421	271	399	288	319	372	344
280	399	274	352	222	305	338	284	216	294	241	315	213	234
277	226	206	297	258	290	232	263	346	329	216	286	333	170
239	368	276	160	208	271	308	250	279	305	208	322	330	245
203	231	238	302	365	428	226	296	263	289	307	348	268	266
186	171	265	243	225	179	293	275	266	243	166	307	230	154

90	100	110	120	130	140	150	160	170	180	Baseline Temperature
289	289	289	289	289	289	289	289	289	289	289

226	224	214	357	226	224	406	214	301	268	284
179	273	343	409	179	273	374	350	431	310	302
268	268	329	350	268	268	340	289	287	319	288
343	235	251	195	343	235	195	284	261	250	275
269	371	304	321	269	371	343	402	237	215	272
211	229	220	192	211	229	315	289	190	326	268
282	278	281	298	282	278	348	246	218	227	269
336	252	260	231	336	252	312	256	318	233	298
271	270	325	244	271	270	253	283	275	309	273
295	243	265	213	295	243	203	297	326	292	272
210	259	257	280	210	259	239	218	238	235	277
289	251	291	297	289	251	267	290	268	291	282
295	286	313	280	295	286	313	264	236	336	294
310	284	243	271	310	284	280	305	278	328	302
306	286	310	318	306	286	334	345	348	325	317
333	317	346	313	333	317	354	351	345	310	334
401	372	372	359	401	372	399	374	399	367	367
423	419	435	410	423	419	430	426	425	396	413
546	528	523	506	546	528	535	552	542	535	536
534	536	559	556	534	536	543	547	535	560	547
609	606	607	596	609	606	635	607	628	593	604
625	638	622	614	625	638	652	605	627	639	640
635	586	601	647	635	586	624	636	595	646	631
574	561	536	584	574	561	598	588	615	589	594
554	499	562	572	554	499	546	595	544	551	543
377	307	313	360	377	307	379	350	316	346	344
412	375	319	325	412	375	364	353	338	338	330
210	274	249	285	210	274	274	325	215	255	295

357	387	383	430	357	387	363	369	397	331	370
327	322	307	254	327	322	425	353	336	275	337
284	226	275	344	284	226	314	271	415	288	322
305	232	312	234	305	232	300	216	266	241	296
290	255	308	170	290	255	352	346	311	216	288
271	350	348	245	271	350	318	279	245	208	298
428	375	258	266	428	375	215	263	330	307	268
179	164	323	154	179	164	293	266	273	166	253

B.4: Pressure Data (bar)

	-180	-170	-160	-150	-140	-130	-120	-110	-100	-90	-80	-70	-60
-180	0.84	0.75	0.80	0.88	0.80	0.77	0.64	0.90	0.82	0.64	0.81	0.75	0.53
-170	0.90	0.76	0.66	0.93	0.93	0.97	1.03	0.90	1.33	1.02	0.83	0.76	1.11
-160	0.87	0.85	0.56	0.91	0.97	1.01	1.00	0.77	0.76	1.27	1.02	0.85	0.89
-150	0.87	0.58	0.87	0.46	0.78	1.08	0.78	0.81	0.57	0.51	1.15	0.58	1.05
-140	0.92	0.82	0.58	0.58	0.69	0.66	0.98	0.68	1.16	1.02	1.00	0.82	1.19
-130	0.91	1.16	0.90	0.73	1.10	1.22	0.74	0.81	0.87	1.04	1.02	1.16	0.81
-120	1.09	1.07	0.94	0.98	0.81	0.93	1.00	0.91	0.97	0.75	0.93	1.07	0.82
-110	1.15	0.56	0.84	1.10	0.89	0.83	1.00	1.15	1.09	1.13	0.97	0.56	1.15
-100	1.18	0.99	1.01	1.05	1.29	1.31	1.36	1.05	0.96	1.10	1.18	0.99	1.17
-90	1.57	1.34	1.25	1.06	1.35	1.37	1.22	1.53	1.35	1.32	1.25	1.34	0.95
-80	1.50	1.52	1.27	1.62	1.22	1.52	1.33	1.55	1.34	1.20	1.64	1.52	1.23
-70	2.22	1.56	1.48	1.88	1.72	1.44	1.72	1.58	1.57	1.80	1.84	1.56	1.55
-60	2.48	2.00	2.01	1.98	2.30	1.92	2.15	2.00	1.85	2.11	2.20	2.00	1.80
-50	2.57	2.46	2.06	2.40	2.64	2.24	1.96	2.62	2.82	2.19	2.26	2.46	2.46
-40	4.34	2.65	3.23	2.78	3.09	3.16	2.95	3.38	2.85	3.19	2.83	2.65	3.18
-30	4.84	3.87	3.54	3.96	3.48	3.49	3.89	4.01	3.74	3.59	3.82	3.87	3.70
-20	5.03	4.64	4.90	4.84	4.76	4.68	4.82	4.65	4.99	5.03	4.64	4.64	5.36
-10	7.60	6.10	5.85	6.07	5.67	5.99	6.23	6.17	5.92	5.75	6.11	6.10	5.89
0	7.96	8.10	7.90	7.81	7.95	8.07	7.76	7.89	7.65	7.96	8.01	8.10	8.21
10	7.52	7.68	7.68	7.77	8.02	8.08	8.00	7.86	7.37	7.69	7.89	7.68	7.61
20	6.98	7.74	8.14	8.17	7.68	7.88	7.86	7.90	7.57	7.65	7.59	7.74	8.03
30	6.89	7.19	7.08	7.34	7.17	7.11	6.98	7.39	7.38	7.15	6.90	7.19	7.04
40	4.12	5.93	5.83	6.33	6.15	5.84	5.72	5.90	5.76	6.03	5.73	5.93	5.85
50	3.78	4.85	4.79	4.70	4.74	4.79	4.31	4.68	4.68	4.61	4.56	4.85	4.71
60	2.96	3.39	3.88	3.50	3.77	3.59	3.85	3.61	3.79	3.85	3.53	3.39	3.65

70	2.02	2.20	2.13	2.61	2.04	2.28	1.85	1.91	1.77	2.18	2.61	2.20	1.72
80	1.71	1.34	1.50	1.47	1.75	1.58	1.65	1.79	1.90	1.64	1.81	1.34	2.02
90	1.39	1.63	1.24	1.26	1.18	1.53	1.15	1.12	1.25	1.48	1.31	1.63	1.27
100	1.30	1.68	1.43	1.45	1.38	1.62	1.60	1.26	1.54	1.25	1.56	1.68	1.38
110	1.27	1.65	1.58	1.34	1.05	1.63	1.18	1.16	1.37	1.30	1.12	1.65	1.52
120	0.93	1.32	0.94	1.02	1.03	1.19	0.98	1.17	1.12	1.17	0.99	1.32	1.16
130	0.88	1.38	1.12	1.21	0.81	1.06	1.05	0.78	0.96	0.76	1.16	1.38	1.25
140	0.91	1.06	0.79	0.95	0.70	1.10	0.99	1.21	0.74	1.11	0.97	1.06	1.12
150	0.76	0.73	0.65	0.65	0.65	0.63	1.08	0.76	0.54	0.76	0.93	0.73	0.59
160	0.80	0.94	0.59	0.91	0.93	0.65	0.78	0.86	0.70	0.80	0.97	0.94	0.65
170	0.78	1.10	0.83	0.75	0.50	1.02	0.97	0.84	0.70	0.92	0.89	1.10	0.68
180	0.82	0.72	1.06	0.72	0.99	0.88	1.01	0.78	0.77	0.80	1.06	0.72	0.81

-50	-40	-30	-20	-10	0	10	20	30	40	50	60	70	80
1.02	0.73	0.57	0.78	0.64	0.67	0.75	1.03	0.64	1.07	0.80	1.24	0.84	1.06
0.92	0.96	0.85	0.75	0.88	0.54	0.84	0.82	1.05	1.13	0.93	0.90	1.16	1.22
0.85	0.89	0.98	0.90	0.59	0.81	1.14	0.91	0.88	0.62	0.97	0.61	0.78	1.06
1.21	0.82	0.80	0.67	0.91	1.07	1.29	1.06	0.88	0.99	0.78	0.64	1.16	0.61
1.10	0.67	0.57	0.94	0.76	0.87	0.68	1.28	1.29	0.99	0.69	0.82	0.89	1.03
1.10	0.73	0.91	0.80	1.08	0.71	0.87	0.71	0.97	0.65	1.10	1.16	0.80	0.65
0.75	0.74	1.26	1.12	1.01	1.01	1.18	1.01	0.88	1.13	0.81	1.33	0.85	1.06
0.70	1.45	0.93	1.09	1.04	1.29	1.10	0.74	0.98	1.37	0.89	1.09	0.91	0.89
1.39	0.95	1.23	1.15	0.80	1.13	1.64	0.79	1.18	1.43	1.29	0.92	1.25	1.02
0.93	1.24	1.45	1.13	1.16	1.36	1.39	1.20	1.37	1.24	1.35	1.28	1.20	0.98
1.42	1.66	1.56	1.51	1.59	1.09	1.64	1.89	1.13	1.46	1.22	1.40	1.26	1.45
1.71	1.61	2.15	1.71	1.61	1.71	1.79	1.77	1.72	1.92	1.72	1.48	1.92	1.76
1.83	1.98	1.74	2.28	2.13	2.02	1.87	2.06	1.81	2.18	2.30	2.16	2.29	1.92

2.15	2.36	2.65	2.62	2.13	2.50	2.53	2.25	2.45	2.60	2.64	2.46	2.35	2.18
3.26	2.78	3.25	2.98	3.00	2.92	3.02	2.68	3.29	3.04	3.09	3.12	3.19	3.03
3.66	3.73	4.11	3.59	3.98	3.73	3.52	3.83	3.94	3.78	3.48	4.18	3.98	3.51
4.54	4.40	4.86	4.77	4.49	5.20	4.87	4.48	4.84	4.83	4.76	4.86	4.82	4.65
5.90	5.96	5.83	6.08	6.21	6.06	5.78	6.09	6.10	5.65	5.67	5.81	6.21	5.87
8.05	7.82	7.92	8.10	8.12	8.11	7.76	7.85	8.20	7.93	7.95	8.04	8.00	7.52
8.10	7.65	7.54	7.92	7.58	7.65	7.67	8.28	7.84	7.43	8.02	8.14	8.02	7.96
7.86	7.98	8.04	8.26	7.74	7.89	7.79	7.91	7.86	8.02	7.68	7.79	8.17	7.71
6.94	7.29	6.58	7.13	7.56	7.01	7.28	7.32	6.78	7.24	7.17	6.97	7.40	6.89
6.12	6.24	5.91	6.02	5.84	6.05	6.40	5.94	6.05	6.02	6.15	6.10	5.99	6.16
4.68	4.80	4.88	4.71	5.04	4.62	4.83	4.42	4.73	4.66	4.74	4.80	4.66	4.70
3.48	3.88	3.61	4.05	3.88	3.79	3.55	3.69	4.08	3.80	3.77	4.02	3.88	3.92
2.08	2.29	2.05	2.05	1.90	2.23	2.43	2.12	2.07	2.02	2.04	2.06	2.06	2.13
1.74	1.88	1.18	1.63	1.66	2.13	1.73	1.43	1.83	1.36	1.75	1.50	1.57	1.68
1.39	1.09	1.35	1.43	1.24	0.97	1.25	1.32	1.50	1.42	1.18	1.64	1.49	1.31
1.74	1.83	1.33	1.46	1.54	1.49	1.32	1.26	1.54	1.27	1.38	1.24	1.35	1.79
1.27	1.88	1.27	1.56	1.24	1.25	0.85	1.47	1.35	1.41	1.05	0.87	1.04	0.97
0.95	1.47	1.24	1.26	1.37	1.01	1.41	1.50	0.97	1.42	1.03	1.14	1.33	1.23
0.94	1.34	0.92	1.19	0.75	1.03	1.14	0.96	0.73	0.99	0.81	1.06	0.72	0.79
0.89	0.73	0.66	0.96	0.83	0.93	0.75	0.85	1.11	1.06	0.70	0.92	1.07	0.55
0.74	1.14	0.86	0.50	0.65	0.84	0.96	0.78	0.87	0.95	0.65	1.00	1.03	0.76
0.62	0.70	0.72	0.92	1.11	1.30	0.69	0.90	0.80	0.88	0.93	1.06	0.81	0.81
0.56	0.51	0.79	0.73	0.67	0.54	0.88	0.82	0.80	0.73	0.50	0.92	0.69	0.46
0.56	0.93	0.66	1.15	0.83	0.61	0.78	0.74	0.92	0.68	0.99	1.04	0.56	0.87

90	100	110	120	130	140	150	160	170	180	Baseline Pressure (bar)
0.67	0.67	0.64	1.06	0.67	0.67	1.21	0.64	0.90	0.80	0.84

0.54	0.82	1.03	1.22	0.54	0.82	1.12	1.05	1.29	0.93	0.90
0.81	0.81	1.00	1.06	0.81	0.81	1.03	0.88	0.87	0.97	0.87
1.07	0.73	0.78	0.61	1.07	0.73	0.61	0.88	0.81	0.78	0.85
0.87	1.19	0.98	1.03	0.87	1.19	1.10	1.29	0.76	0.69	0.87
0.71	0.77	0.74	0.65	0.71	0.77	1.06	0.97	0.64	1.10	0.90
1.01	0.99	1.00	1.06	1.01	0.99	1.24	0.88	0.78	0.81	0.96
1.29	0.97	1.00	0.89	1.29	0.97	1.20	0.98	1.22	0.89	1.14
1.13	1.13	1.36	1.02	1.13	1.13	1.06	1.18	1.15	1.29	1.14
1.36	1.12	1.22	0.98	1.36	1.12	0.94	1.37	1.50	1.35	1.25
1.09	1.34	1.33	1.45	1.09	1.34	1.24	1.13	1.23	1.22	1.43
1.71	1.48	1.72	1.76	1.71	1.48	1.58	1.72	1.58	1.72	1.67
2.02	1.96	2.15	1.92	2.02	1.96	2.14	1.81	1.62	2.30	2.02
2.50	2.28	1.96	2.18	2.50	2.28	2.25	2.45	2.24	2.64	2.43
2.92	2.72	2.95	3.03	2.92	2.72	3.18	3.29	3.32	3.09	3.01
3.73	3.55	3.89	3.51	3.73	3.55	3.98	3.94	3.87	3.48	3.75
5.20	4.82	4.82	4.65	5.20	4.82	5.16	4.84	5.17	4.76	4.76
6.06	6.00	6.23	5.87	6.06	6.00	6.16	6.10	6.09	5.67	5.91
8.11	7.84	7.76	7.52	8.11	7.84	7.95	8.20	8.04	7.95	7.96
7.65	7.67	8.00	7.96	7.65	7.67	7.78	7.84	7.66	8.02	7.82
7.89	7.85	7.86	7.71	7.89	7.85	8.23	7.86	8.14	7.68	7.82
7.01	7.16	6.98	6.89	7.01	7.16	7.32	6.78	7.03	7.17	7.18
6.05	5.58	5.72	6.16	6.05	5.58	5.94	6.05	5.67	6.15	6.00
4.62	4.51	4.31	4.70	4.62	4.51	4.81	4.73	4.95	4.74	4.78
3.79	3.42	3.85	3.92	3.79	3.42	3.74	4.08	3.73	3.77	3.72
2.23	1.81	1.85	2.13	2.23	1.81	2.24	2.07	1.87	2.04	2.03
2.13	1.94	1.65	1.68	2.13	1.94	1.88	1.83	1.75	1.75	1.71
0.97	1.26	1.15	1.31	0.97	1.26	1.26	1.50	0.99	1.18	1.36
1.49	1.61	1.60	1.79	1.49	1.61	1.51	1.54	1.66	1.38	1.54

1.25	1.23	1.18	0.97	1.25	1.23	1.63	1.35	1.29	1.05	1.29
1.01	0.81	0.98	1.23	1.01	0.81	1.12	0.97	1.48	1.03	1.15
1.03	0.78	1.05	0.79	1.03	0.78	1.01	0.73	0.90	0.81	1.00
0.93	0.82	0.99	0.55	0.93	0.82	1.13	1.11	1.00	0.70	0.92
0.84	1.09	1.08	0.76	0.84	1.09	0.99	0.87	0.76	0.65	0.92
1.30	1.14	0.78	0.81	1.30	1.14	0.65	0.80	1.00	0.93	0.81
0.54	0.49	0.97	0.46	0.54	0.49	0.88	0.80	0.82	0.50	0.76
0.61	0.59	1.01	0.87	0.61	0.59	0.52	0.92	0.63	0.99	0.82

B.5: Frequency (GHz)

Frequency	-180	-170	-160	-150	-140	-130	-120	-110
-180	2.44E+09	2.44E+09	2.44E+09	2.44E+09	2.44E+09	2.44E+09	2.45E+09	2.44E+09
-170	2.44E+09	2.44E+09	2.44E+09	2.44E+09	2.44E+09	2.44E+09	2.44E+09	2.44E+09
-160	2.44E+09	2.44E+09	2.44E+09	2.44E+09	2.44E+09	2.44E+09	2.44E+09	2.44E+09
-150	2.44E+09	2.45E+09	2.44E+09	2.45E+09	2.44E+09	2.44E+09	2.44E+09	2.44E+09
-140	2.44E+09	2.44E+09	2.45E+09	2.44E+09	2.44E+09	2.45E+09	2.44E+09	2.44E+09
-130	2.44E+09	2.44E+09	2.44E+09	2.44E+09	2.44E+09	2.44E+09	2.44E+09	2.44E+09
-120	2.44E+09	2.44E+09	2.44E+09	2.44E+09	2.44E+09	2.44E+09	2.44E+09	2.44E+09
-110	2.44E+09	2.45E+09	2.44E+09	2.44E+09	2.44E+09	2.44E+09	2.44E+09	2.44E+09
-100	2.44E+09	2.44E+09	2.44E+09	2.44E+09	2.44E+09	2.44E+09	2.44E+09	2.44E+09
-90	2.44E+09	2.44E+09	2.44E+09	2.44E+09	2.44E+09	2.44E+09	2.44E+09	2.44E+09
-80	2.44E+09	2.44E+09	2.44E+09	2.44E+09	2.44E+09	2.44E+09	2.44E+09	2.44E+09
-70	2.43E+09	2.44E+09	2.44E+09	2.44E+09	2.43E+09	2.44E+09	2.44E+09	2.44E+09
-60	2.44E+09	2.43E+09	2.43E+09	2.44E+09	2.43E+09	2.43E+09	2.43E+09	2.43E+09
-50	2.44E+09	2.43E+09	2.44E+09	2.43E+09	2.43E+09	2.43E+09	2.44E+09	2.43E+09
-40	2.42E+09	2.43E+09	2.42E+09	2.43E+09	2.43E+09	2.43E+09	2.42E+09	2.43E+09
-30	2.43E+09	2.42E+09	2.43E+09	2.42E+09	2.43E+09	2.43E+09	2.42E+09	2.43E+09
-20	2.43E+09	2.42E+09	2.42E+09	2.42E+09	2.42E+09	2.42E+09	2.42E+09	2.42E+09
-10	2.41E+09	2.41E+09	2.42E+09	2.42E+09	2.42E+09	2.42E+09	2.42E+09	2.41E+09
0	2.42E+09	2.41E+09	2.41E+09	2.41E+09	2.41E+09	2.41E+09	2.41E+09	2.41E+09
10	2.42E+09	2.42E+09	2.42E+09	2.42E+09	2.42E+09	2.42E+09	2.42E+09	2.42E+09
20	2.42E+09	2.42E+09	2.42E+09	2.42E+09	2.42E+09	2.42E+09	2.42E+09	2.42E+09
30	2.42E+09	2.42E+09	2.43E+09	2.43E+09	2.42E+09	2.43E+09	2.43E+09	2.42E+09
40	2.44E+09	2.43E+09	2.43E+09	2.43E+09	2.43E+09	2.43E+09	2.43E+09	2.43E+09
50	2.43E+09	2.43E+09	2.43E+09	2.44E+09	2.43E+09	2.43E+09	2.43E+09	2.43E+09
60	2.44E+09	2.44E+09	2.44E+09	2.44E+09	2.44E+09	2.44E+09	2.43E+09	2.44E+09

70	2.44E+09	2.44E+09	2.44E+09	2.44E+09	2.44E+09	2.44E+09	2.44E+09	2.44E+09
80	2.44E+09	2.44E+09	2.44E+09	2.44E+09	2.44E+09	2.44E+09	2.44E+09	2.44E+09
90	2.44E+09	2.44E+09	2.44E+09	2.44E+09	2.44E+09	2.44E+09	2.44E+09	2.44E+09
100	2.44E+09	2.44E+09	2.44E+09	2.44E+09	2.44E+09	2.44E+09	2.44E+09	2.44E+09
110	2.44E+09	2.44E+09	2.44E+09	2.44E+09	2.44E+09	2.44E+09	2.44E+09	2.44E+09
120	2.44E+09	2.44E+09	2.45E+09	2.44E+09	2.44E+09	2.44E+09	2.44E+09	2.44E+09
130	2.44E+09	2.44E+09	2.44E+09	2.44E+09	2.44E+09	2.44E+09	2.44E+09	2.44E+09
140	2.44E+09	2.44E+09	2.44E+09	2.44E+09	2.44E+09	2.44E+09	2.44E+09	2.44E+09
150	2.44E+09	2.45E+09	2.44E+09	2.45E+09	2.44E+09	2.45E+09	2.44E+09	2.45E+09
160	2.44E+09	2.44E+09	2.44E+09	2.44E+09	2.44E+09	2.44E+09	2.45E+09	2.44E+09
170	2.44E+09	2.44E+09	2.44E+09	2.44E+09	2.45E+09	2.44E+09	2.44E+09	2.44E+09
180	2.44E+09	2.45E+09	2.44E+09	2.44E+09	2.44E+09	2.44E+09	2.44E+09	2.44E+09

-100	-90	-80	-70	-60	-50	-40	-30	-20
2.44E+09	2.45E+09	2.44E+09	2.44E+09	2.45E+09	2.44E+09	2.44E+09	2.45E+09	2.44E+09
2.44E+09	2.44E+09	2.44E+09	2.44E+09	2.44E+09	2.44E+09	2.44E+09	2.44E+09	2.44E+09
2.45E+09	2.44E+09	2.44E+09	2.44E+09	2.44E+09	2.44E+09	2.44E+09	2.44E+09	2.44E+09
2.45E+09	2.45E+09	2.44E+09	2.45E+09	2.44E+09	2.44E+09	2.44E+09	2.44E+09	2.45E+09
2.44E+09	2.44E+09	2.44E+09	2.44E+09	2.44E+09	2.44E+09	2.44E+09	2.45E+09	2.44E+09
2.44E+09	2.44E+09	2.44E+09	2.44E+09	2.45E+09	2.44E+09	2.44E+09	2.44E+09	2.44E+09
2.44E+09	2.44E+09	2.44E+09	2.44E+09	2.44E+09	2.45E+09	2.44E+09	2.44E+09	2.44E+09
2.44E+09	2.44E+09	2.44E+09	2.45E+09	2.44E+09	2.44E+09	2.44E+09	2.44E+09	2.44E+09
2.44E+09	2.44E+09	2.44E+09	2.44E+09	2.44E+09	2.43E+09	2.44E+09	2.44E+09	2.44E+09
2.44E+09	2.44E+09	2.44E+09	2.44E+09	2.44E+09	2.44E+09	2.44E+09	2.44E+09	2.44E+09
2.44E+09	2.44E+09	2.44E+09	2.44E+09	2.44E+09	2.44E+09	2.44E+09	2.44E+09	2.44E+09
2.44E+09	2.43E+09	2.44E+09	2.44E+09	2.44E+09	2.44E+09	2.44E+09	2.43E+09	2.44E+09
2.44E+09	2.44E+09	2.44E+09	2.43E+09	2.44E+09	2.44E+09	2.43E+09	2.44E+09	2.43E+09

2.43E+09	2.44E+09	2.44E+09	2.43E+09	2.43E+09	2.43E+09	2.43E+09	2.43E+09	2.43E+09
2.43E+09	2.43E+09	2.43E+09	2.43E+09	2.43E+09	2.42E+09	2.43E+09	2.43E+09	2.43E+09
2.42E+09	2.43E+09	2.42E+09	2.42E+09	2.43E+09	2.43E+09	2.42E+09	2.42E+09	2.43E+09
2.42E+09	2.42E+09	2.42E+09	2.42E+09	2.42E+09	2.42E+09	2.42E+09	2.42E+09	2.42E+09
2.42E+09	2.42E+09	2.41E+09	2.41E+09	2.42E+09	2.41E+09	2.41E+09	2.42E+09	2.42E+09
2.41E+09	2.41E+09	2.41E+09	2.41E+09	2.41E+09	2.41E+09	2.41E+09	2.41E+09	2.41E+09
2.42E+09	2.42E+09	2.42E+09	2.42E+09	2.42E+09	2.42E+09	2.42E+09	2.42E+09	2.42E+09
2.42E+09	2.42E+09	2.42E+09	2.42E+09	2.42E+09	2.42E+09	2.42E+09	2.42E+09	2.42E+09
2.42E+09	2.42E+09	2.43E+09	2.42E+09	2.43E+09	2.43E+09	2.43E+09	2.43E+09	2.43E+09
2.43E+09	2.43E+09	2.43E+09	2.43E+09	2.43E+09	2.43E+09	2.43E+09	2.43E+09	2.43E+09
2.43E+09	2.43E+09	2.43E+09	2.43E+09	2.43E+09	2.43E+09	2.43E+09	2.43E+09	2.43E+09
2.44E+09	2.44E+09	2.44E+09	2.44E+09	2.44E+09	2.44E+09	2.44E+09	2.44E+09	2.44E+09
2.44E+09	2.44E+09	2.44E+09	2.44E+09	2.44E+09	2.44E+09	2.44E+09	2.44E+09	2.44E+09
2.44E+09	2.44E+09	2.44E+09	2.44E+09	2.44E+09	2.44E+09	2.44E+09	2.44E+09	2.44E+09
2.44E+09	2.44E+09	2.44E+09	2.44E+09	2.44E+09	2.44E+09	2.44E+09	2.44E+09	2.44E+09
2.44E+09	2.44E+09	2.44E+09	2.44E+09	2.44E+09	2.44E+09	2.43E+09	2.44E+09	2.44E+09
2.44E+09	2.44E+09	2.44E+09	2.44E+09	2.44E+09	2.44E+09	2.44E+09	2.44E+09	2.44E+09
2.44E+09	2.44E+09	2.44E+09	2.44E+09	2.44E+09	2.44E+09	2.44E+09	2.44E+09	2.44E+09
2.44E+09	2.45E+09	2.44E+09	2.44E+09	2.44E+09	2.44E+09	2.44E+09	2.44E+09	2.44E+09
2.44E+09	2.44E+09	2.44E+09	2.44E+09	2.44E+09	2.44E+09	2.45E+09	2.44E+09	2.44E+09
2.45E+09	2.45E+09	2.44E+09	2.45E+09	2.45E+09	2.44E+09	2.44E+09	2.44E+09	2.45E+09
2.44E+09	2.44E+09	2.44E+09	2.44E+09	2.44E+09	2.44E+09	2.45E+09	2.44E+09	2.44E+09
2.44E+09	2.44E+09	2.44E+09	2.44E+09	2.44E+09	2.44E+09	2.45E+09	2.44E+09	2.44E+09
2.44E+09	2.44E+09	2.44E+09	2.45E+09	2.44E+09	2.44E+09	2.44E+09	2.44E+09	2.44E+09

-10	0	10	20	30	40	50	60	70
2.45E+09	2.45E+09	2.44E+09	2.44E+09	2.45E+09	2.44E+09	2.44E+09	2.44E+09	2.44E+09

2.44E+09	2.44E+09	2.44E+09	2.44E+09	2.44E+09	2.44E+09	2.44E+09	2.45E+09	2.44E+09
2.45E+09	2.44E+09	2.44E+09	2.44E+09	2.44E+09	2.45E+09	2.44E+09	2.45E+09	2.45E+09
2.44E+09	2.44E+09	2.44E+09	2.44E+09	2.44E+09	2.44E+09	2.44E+09	2.44E+09	2.44E+09
2.44E+09	2.44E+09	2.45E+09	2.44E+09	2.44E+09	2.44E+09	2.44E+09	2.44E+09	2.44E+09
2.44E+09	2.44E+09	2.44E+09	2.45E+09	2.44E+09	2.45E+09	2.44E+09	2.44E+09	2.44E+09
2.44E+09	2.44E+09	2.44E+09	2.44E+09	2.44E+09	2.44E+09	2.44E+09	2.44E+09	2.44E+09
2.44E+09	2.44E+09	2.44E+09	2.44E+09	2.44E+09	2.44E+09	2.44E+09	2.44E+09	2.44E+09
2.44E+09	2.44E+09	2.44E+09	2.44E+09	2.44E+09	2.44E+09	2.44E+09	2.44E+09	2.44E+09
2.44E+09	2.44E+09	2.44E+09	2.44E+09	2.44E+09	2.44E+09	2.44E+09	2.44E+09	2.44E+09
2.44E+09	2.44E+09	2.44E+09	2.43E+09	2.44E+09	2.44E+09	2.44E+09	2.44E+09	2.44E+09
2.44E+09	2.43E+09	2.44E+09	2.44E+09	2.43E+09	2.44E+09	2.43E+09	2.44E+09	2.43E+09
2.43E+09	2.44E+09	2.44E+09	2.44E+09	2.44E+09	2.44E+09	2.43E+09	2.43E+09	2.44E+09
2.44E+09	2.43E+09	2.43E+09	2.43E+09	2.43E+09	2.43E+09	2.43E+09	2.43E+09	2.44E+09
2.43E+09	2.43E+09	2.43E+09	2.43E+09	2.43E+09	2.43E+09	2.43E+09	2.43E+09	2.43E+09
2.42E+09	2.42E+09	2.43E+09	2.42E+09	2.43E+09	2.43E+09	2.43E+09	2.42E+09	2.43E+09
2.42E+09	2.42E+09	2.42E+09	2.42E+09	2.42E+09	2.42E+09	2.42E+09	2.42E+09	2.42E+09
2.41E+09	2.42E+09	2.42E+09	2.41E+09	2.42E+09	2.42E+09	2.42E+09	2.42E+09	2.42E+09
2.41E+09	2.41E+09	2.41E+09	2.41E+09	2.41E+09	2.41E+09	2.41E+09	2.41E+09	2.41E+09
2.42E+09	2.42E+09	2.42E+09	2.42E+09	2.42E+09	2.42E+09	2.42E+09	2.42E+09	2.42E+09
2.42E+09	2.42E+09	2.42E+09	2.42E+09	2.42E+09	2.42E+09	2.42E+09	2.42E+09	2.42E+09
2.42E+09	2.43E+09	2.42E+09	2.42E+09	2.43E+09	2.43E+09	2.42E+09	2.43E+09	2.43E+09
2.43E+09	2.43E+09	2.43E+09	2.43E+09	2.43E+09	2.43E+09	2.43E+09	2.43E+09	2.43E+09
2.43E+09	2.43E+09	2.43E+09	2.44E+09	2.43E+09	2.43E+09	2.43E+09	2.43E+09	2.43E+09
2.44E+09	2.44E+09	2.44E+09	2.44E+09	2.44E+09	2.44E+09	2.44E+09	2.44E+09	2.44E+09
2.44E+09	2.44E+09	2.44E+09	2.44E+09	2.44E+09	2.44E+09	2.44E+09	2.44E+09	2.44E+09
2.44E+09	2.44E+09	2.44E+09	2.44E+09	2.44E+09	2.44E+09	2.44E+09	2.44E+09	2.44E+09
2.44E+09	2.45E+09	2.44E+09	2.44E+09	2.44E+09	2.44E+09	2.44E+09	2.44E+09	2.44E+09
2.44E+09	2.44E+09	2.44E+09	2.44E+09	2.44E+09	2.44E+09	2.44E+09	2.44E+09	2.44E+09

2.44E+09	2.44E+09	2.44E+09	2.44E+09	2.44E+09	2.44E+09	2.44E+09	2.44E+09	2.44E+09
2.44E+09	2.44E+09	2.44E+09	2.44E+09	2.44E+09	2.44E+09	2.44E+09	2.44E+09	2.44E+09
2.45E+09	2.44E+09	2.44E+09	2.45E+09	2.44E+09	2.44E+09	2.44E+09	2.44E+09	2.45E+09
2.44E+09	2.44E+09	2.45E+09	2.44E+09	2.44E+09	2.44E+09	2.44E+09	2.44E+09	2.44E+09
2.44E+09	2.44E+09	2.44E+09	2.44E+09	2.44E+09	2.44E+09	2.44E+09	2.44E+09	2.44E+09
2.44E+09	2.44E+09	2.45E+09	2.44E+09	2.44E+09	2.44E+09	2.44E+09	2.44E+09	2.44E+09
2.45E+09	2.45E+09	2.44E+09	2.44E+09	2.44E+09	2.44E+09	2.45E+09	2.44E+09	2.44E+09
2.44E+09	2.44E+09	2.44E+09	2.44E+09	2.44E+09	2.44E+09	2.44E+09	2.44E+09	2.44E+09

80	90	100	110	120	130	140	150	160
2.44E+09	2.45E+09	2.45E+09	2.45E+09	2.44E+09	2.45E+09	2.45E+09	2.44E+09	2.45E+09
2.44E+09	2.44E+09	2.44E+09	2.44E+09	2.44E+09	2.44E+09	2.44E+09	2.44E+09	2.44E+09
2.44E+09	2.44E+09	2.44E+09	2.44E+09	2.44E+09	2.44E+09	2.44E+09	2.44E+09	2.44E+09
2.45E+09	2.44E+09	2.44E+09	2.44E+09	2.45E+09	2.44E+09	2.44E+09	2.45E+09	2.44E+09
2.44E+09	2.44E+09	2.44E+09	2.44E+09	2.44E+09	2.44E+09	2.44E+09	2.44E+09	2.44E+09
2.45E+09	2.44E+09	2.45E+09	2.44E+09	2.45E+09	2.44E+09	2.45E+09	2.44E+09	2.44E+09
2.44E+09	2.44E+09	2.44E+09	2.44E+09	2.44E+09	2.44E+09	2.44E+09	2.44E+09	2.44E+09
2.44E+09	2.44E+09	2.44E+09	2.44E+09	2.44E+09	2.44E+09	2.44E+09	2.44E+09	2.44E+09
2.44E+09	2.44E+09	2.44E+09	2.44E+09	2.44E+09	2.44E+09	2.44E+09	2.44E+09	2.44E+09
2.44E+09	2.44E+09	2.44E+09	2.44E+09	2.44E+09	2.44E+09	2.44E+09	2.44E+09	2.44E+09
2.44E+09	2.44E+09	2.44E+09	2.44E+09	2.44E+09	2.44E+09	2.44E+09	2.44E+09	2.44E+09
2.44E+09	2.43E+09	2.44E+09	2.44E+09	2.44E+09	2.43E+09	2.44E+09	2.44E+09	2.43E+09
2.44E+09	2.44E+09	2.43E+09	2.43E+09	2.44E+09	2.44E+09	2.43E+09	2.43E+09	2.44E+09
2.43E+09	2.43E+09	2.43E+09	2.44E+09	2.43E+09	2.43E+09	2.43E+09	2.43E+09	2.43E+09
2.43E+09	2.43E+09	2.43E+09	2.42E+09	2.43E+09	2.43E+09	2.43E+09	2.43E+09	2.43E+09
2.43E+09	2.42E+09	2.42E+09	2.42E+09	2.43E+09	2.42E+09	2.42E+09	2.43E+09	2.43E+09
2.42E+09	2.42E+09	2.42E+09	2.42E+09	2.42E+09	2.42E+09	2.42E+09	2.42E+09	2.42E+09

2.42E+09	2.42E+09	2.42E+09	2.42E+09	2.42E+09	2.42E+09	2.42E+09	2.42E+09	2.42E+09
2.41E+09	2.41E+09	2.41E+09	2.41E+09	2.41E+09	2.41E+09	2.41E+09	2.41E+09	2.41E+09
2.42E+09	2.42E+09	2.42E+09	2.42E+09	2.42E+09	2.42E+09	2.42E+09	2.42E+09	2.42E+09
2.42E+09	2.42E+09	2.42E+09	2.42E+09	2.42E+09	2.42E+09	2.42E+09	2.42E+09	2.42E+09
2.43E+09	2.43E+09	2.43E+09	2.43E+09	2.43E+09	2.43E+09	2.43E+09	2.43E+09	2.43E+09
2.43E+09	2.43E+09	2.43E+09	2.43E+09	2.43E+09	2.43E+09	2.43E+09	2.43E+09	2.43E+09
2.43E+09	2.43E+09	2.43E+09	2.43E+09	2.43E+09	2.43E+09	2.43E+09	2.43E+09	2.43E+09
2.44E+09	2.44E+09	2.44E+09	2.43E+09	2.44E+09	2.44E+09	2.44E+09	2.44E+09	2.44E+09
2.44E+09	2.44E+09	2.44E+09	2.44E+09	2.44E+09	2.44E+09	2.44E+09	2.44E+09	2.44E+09
2.44E+09	2.44E+09	2.44E+09	2.44E+09	2.44E+09	2.44E+09	2.44E+09	2.44E+09	2.44E+09
2.44E+09	2.45E+09	2.44E+09	2.44E+09	2.44E+09	2.45E+09	2.44E+09	2.44E+09	2.44E+09
2.44E+09	2.44E+09	2.44E+09	2.44E+09	2.44E+09	2.44E+09	2.44E+09	2.44E+09	2.44E+09
2.45E+09	2.44E+09	2.44E+09	2.44E+09	2.45E+09	2.44E+09	2.44E+09	2.44E+09	2.44E+09
2.44E+09	2.44E+09	2.44E+09	2.44E+09	2.44E+09	2.44E+09	2.44E+09	2.44E+09	2.44E+09
2.45E+09	2.44E+09	2.44E+09	2.44E+09	2.45E+09	2.44E+09	2.44E+09	2.44E+09	2.44E+09
2.45E+09	2.44E+09	2.44E+09	2.44E+09	2.45E+09	2.44E+09	2.44E+09	2.44E+09	2.44E+09
2.44E+09	2.44E+09	2.44E+09	2.44E+09	2.44E+09	2.44E+09	2.44E+09	2.44E+09	2.44E+09
2.44E+09	2.44E+09	2.44E+09	2.45E+09	2.44E+09	2.44E+09	2.44E+09	2.45E+09	2.44E+09
2.45E+09	2.45E+09	2.45E+09	2.44E+09	2.45E+09	2.45E+09	2.45E+09	2.44E+09	2.44E+09
2.44E+09	2.44E+09	2.44E+09	2.44E+09	2.44E+09	2.44E+09	2.44E+09	2.45E+09	2.44E+09

170	180	Baseline Frequency
2.44E+09	2.44E+09	2.44E+09
2.44E+09	2.44E+09	2.44E+09
2.45E+09	2.44E+09	2.44E+09
2.44E+09	2.44E+09	2.44E+09
2.44E+09	2.44E+09	2.44E+09

2.44E+09	2.44E+09	2.44E+09
2.44E+09	2.44E+09	2.44E+09
2.44E+09	2.44E+09	2.44E+09
2.44E+09	2.44E+09	2.44E+09
2.44E+09	2.44E+09	2.44E+09
2.44E+09	2.44E+09	2.44E+09
2.44E+09	2.43E+09	2.44E+09
2.44E+09	2.43E+09	2.43E+09
2.43E+09	2.43E+09	2.43E+09
2.43E+09	2.43E+09	2.43E+09
2.43E+09	2.43E+09	2.43E+09
2.42E+09	2.42E+09	2.42E+09
2.42E+09	2.42E+09	2.42E+09
2.41E+09	2.41E+09	2.41E+09
2.42E+09	2.42E+09	2.42E+09
2.42E+09	2.42E+09	2.42E+09
2.43E+09	2.42E+09	2.43E+09
2.43E+09	2.43E+09	2.43E+09
2.43E+09	2.43E+09	2.43E+09
2.44E+09	2.44E+09	2.44E+09
2.44E+09	2.44E+09	2.44E+09
2.44E+09	2.44E+09	2.44E+09
2.44E+09	2.44E+09	2.44E+09
2.43E+09	2.44E+09	2.44E+09
2.44E+09	2.44E+09	2.44E+09
2.44E+09	2.44E+09	2.44E+09
2.45E+09	2.44E+09	2.44E+09
2.44E+09	2.44E+09	2.44E+09

2.44E+09	2.44E+09	2.44E+09
2.44E+09	2.44E+09	2.44E+09
2.44E+09	2.45E+09	2.44E+09
2.45E+09	2.44E+09	2.44E+09

B.6: Density

	-180	-170	-160	-150	-140	-130	-120	-110
-180	1.018	0.905	0.959	1.062	0.959	0.923	0.766	1.086
-170	1.102	1.049	0.853	1.088	1.204	1.312	1.670	1.035
-160	1.009	1.156	0.889	1.023	1.085	1.077	1.009	0.889
-150	1.056	0.724	1.638	0.533	0.847	1.128	0.827	1.109
-140	1.137	1.528	0.714	1.351	0.962	0.663	1.351	0.900
-130	1.109	1.576	1.751	1.410	1.775	2.059	0.849	1.342
-120	1.400	1.080	1.223	1.575	0.866	0.892	1.583	1.316
-110	1.308	0.653	1.102	1.400	1.364	1.107	1.235	1.568
-100	1.368	2.343	1.611	1.272	1.923	2.107	1.814	1.216
-90	1.936	1.966	1.788	1.457	1.518	1.523	1.306	2.107
-80	1.527	1.826	1.636	2.455	1.449	1.773	1.748	1.630
-70	2.673	1.843	2.092	2.091	2.550	1.712	2.330	1.830
-60	2.295	2.639	2.803	2.166	2.750	2.742	2.565	2.612
-50	2.474	2.941	2.438	2.898	2.732	2.776	2.174	3.118
-40	4.723	3.012	4.404	3.245	3.285	3.955	4.228	3.616
-30	3.697	4.843	3.627	4.715	3.733	3.666	4.365	3.933
-20	4.060	4.690	5.415	4.781	5.338	5.233	4.842	4.536
-10	6.816	5.925	5.380	5.652	5.373	5.774	5.836	5.980
0	5.224	6.623	6.740	6.422	6.998	6.724	6.212	6.382

10	4.885	4.904	5.025	5.145	5.214	5.178	5.332	5.149
20	4.634	5.029	5.286	5.244	4.778	4.860	4.897	5.015
30	4.452	4.190	3.925	4.052	4.208	4.069	4.008	4.219
40	2.332	3.222	3.214	3.369	3.351	3.211	3.202	3.117
50	3.045	2.708	2.726	2.461	2.557	2.716	2.497	2.629
60	2.193	1.957	2.266	2.083	2.228	2.099	2.503	2.163
70	1.628	1.547	1.311	1.778	1.291	1.517	1.146	1.262
80	1.737	1.256	1.444	1.157	1.764	1.421	1.834	1.922
90	1.468	2.191	1.494	1.543	1.209	1.750	1.250	1.130
100	1.497	1.653	1.849	1.846	1.883	1.698	2.234	1.804
110	1.413	1.425	1.598	1.345	1.104	1.460	1.069	1.330
120	0.984	1.066	0.791	1.014	1.301	0.969	1.111	1.344
130	1.174	1.297	1.480	1.472	0.981	1.110	1.330	0.826
140	1.205	0.900	0.825	0.919	1.005	1.210	1.104	1.828
150	0.933	0.770	0.926	0.760	1.038	0.644	1.220	0.703
160	1.136	1.384	0.972	1.524	1.558	1.115	0.780	1.223
170	1.030	1.235	1.496	0.869	0.561	1.655	1.305	1.030
180	1.098	0.679	1.321	0.991	2.069	0.897	1.088	0.959

-100	-90	-80	-70	-60	-50	-40	-30	-20
0.990	0.766	0.978	0.905	0.640	1.225	0.875	0.688	0.935
1.672	1.662	1.060	1.049	2.157	0.933	1.363	1.534	0.995
0.596	1.294	1.271	1.156	0.833	0.960	0.969	1.200	1.256
0.784	0.424	1.195	0.724	1.251	1.510	0.972	0.865	0.785
2.209	2.150	0.940	1.528	1.225	0.978	0.883	0.763	1.516
0.838	1.141	1.141	1.576	0.761	1.124	1.210	1.802	0.952

1.307	0.849	1.068	1.080	1.186	0.793	1.195	1.615	1.640
1.395	1.870	1.288	0.653	1.733	1.158	2.432	0.920	1.208
1.173	1.297	1.629	2.343	1.361	2.664	0.873	1.755	1.399
2.043	1.741	1.537	1.966	1.172	0.965	1.886	1.711	1.432
1.592	1.452	2.104	1.826	2.087	2.462	2.155	1.726	2.136
2.118	2.713	2.016	1.843	2.263	2.163	1.742	2.491	2.041
2.423	2.405	2.466	2.639	2.396	2.201	2.537	1.664	2.750
3.629	2.476	2.450	2.941	3.259	2.810	2.843	3.632	2.741
2.831	4.084	3.508	3.012	3.622	4.242	3.300	3.436	3.187
4.351	3.736	4.468	4.843	3.856	3.727	4.441	4.186	3.987
5.214	5.474	4.752	4.690	5.660	4.846	4.610	4.621	5.198
5.356	5.151	5.939	5.925	4.952	5.861	6.111	5.416	5.744
6.444	6.910	6.534	6.623	6.953	6.804	6.545	6.770	6.645
4.983	4.993	5.094	4.904	4.797	5.204	5.063	4.924	5.060
5.119	4.964	4.800	5.029	5.259	4.836	5.199	5.318	5.198
4.400	4.213	4.100	4.190	3.954	3.982	4.123	3.694	3.893
3.047	3.294	3.244	3.222	3.249	3.448	3.341	3.506	3.301
2.695	2.536	2.635	2.708	2.666	2.532	2.552	2.739	2.590
2.266	2.340	2.168	1.957	2.170	2.085	2.262	2.070	2.409
1.112	1.350	1.763	1.547	1.125	1.422	1.409	1.356	1.209
2.208	1.543	1.425	1.256	2.409	1.725	1.684	1.184	1.635
1.188	1.625	1.307	2.191	1.135	1.434	1.047	2.053	1.580
1.969	1.359	1.904	1.653	1.743	2.015	2.685	1.586	1.637
1.295	1.503	1.045	1.425	1.598	1.055	1.490	1.385	1.545
1.084	1.198	1.178	1.066	1.012	1.000	1.044	1.296	1.075
1.068	0.810	1.454	1.297	1.338	1.228	1.131	0.924	1.172
0.903	1.710	0.979	0.900	1.054	1.109	0.634	0.840	0.944

0.816	0.766	1.067	0.770	0.589	0.930	1.759	1.449	0.580
1.391	1.137	1.127	1.384	1.181	0.898	0.663	0.910	1.997
1.055	1.206	0.967	1.235	1.104	0.952	0.768	1.157	0.836
1.152	0.909	1.245	0.679	1.240	1.040	1.886	0.862	1.642

-10	0	10	20	30	40	50	60	70	80
0.766	0.809	0.899	1.237	0.766	1.291	0.959	1.490	1.008	1.279
1.434	0.826	1.160	0.823	1.703	1.093	1.204	0.754	1.437	1.191
0.691	1.574	1.419	1.161	0.871	0.570	1.085	0.699	0.699	0.903
1.641	1.387	1.193	1.228	1.061	1.684	0.847	1.107	1.562	0.602
0.896	0.878	0.565	1.300	1.584	1.081	0.962	1.387	0.833	1.840
1.600	0.918	1.442	0.623	0.841	0.734	1.775	1.592	1.006	0.701
1.095	1.658	1.588	1.666	1.056	2.027	0.866	1.338	1.244	1.925
1.272	1.587	1.152	0.909	1.390	1.511	1.364	1.016	1.329	1.036
1.030	1.172	1.989	1.422	1.604	1.386	1.923	1.130	1.823	1.528
2.094	1.746	1.233	2.203	1.678	1.262	1.518	2.010	1.392	1.401
2.208	1.279	1.886	2.526	1.322	1.888	1.449	1.755	1.691	2.373
1.818	2.831	1.972	1.682	2.746	2.369	2.550	1.911	2.745	2.180
2.723	2.437	2.149	2.400	2.165	2.335	2.750	2.995	2.453	2.250
2.385	2.946	3.220	2.605	3.237	2.839	2.732	2.717	2.447	2.708
3.949	3.273	3.351	3.337	3.756	3.277	3.285	3.555	3.797	3.894
4.405	4.241	3.863	4.737	3.975	4.123	3.733	4.448	4.137	3.840
4.403	5.441	5.400	4.570	4.799	4.994	5.338	4.538	4.732	5.170
6.245	5.261	5.359	6.126	5.680	5.281	5.373	5.393	5.812	5.695
6.517	6.670	6.695	6.429	6.709	6.995	6.998	6.907	6.430	6.390
4.828	4.882	5.109	5.459	4.942	4.846	5.214	5.233	5.185	5.475

5.096	5.143	5.065	4.764	5.003	5.383	4.778	4.775	5.080	4.833
4.405	4.007	4.215	4.174	3.891	4.074	4.208	4.033	4.082	4.028
3.015	3.369	3.437	3.170	3.486	3.249	3.351	3.419	3.165	3.495
2.863	2.533	2.501	2.464	2.589	2.563	2.557	2.610	2.576	2.526
2.154	2.298	2.059	2.342	2.416	2.284	2.228	2.343	2.332	2.336
1.166	1.400	1.633	1.370	1.209	1.266	1.291	1.221	1.265	1.295
1.796	1.969	1.464	1.387	1.818	1.383	1.764	1.501	1.571	1.626
1.344	0.816	1.296	1.663	1.476	1.888	1.209	1.969	1.710	1.405
1.993	2.468	1.700	1.525	1.647	1.429	1.883	1.212	1.448	2.191
1.172	1.221	0.929	1.699	1.276	1.611	1.104	1.018	1.122	0.786
1.467	1.076	2.223	1.359	0.952	1.346	1.301	1.738	1.697	1.682
0.677	1.259	0.999	0.790	0.932	0.865	0.981	1.159	0.670	0.795
1.305	1.063	0.769	1.036	1.793	1.248	1.005	1.016	1.753	0.813
0.869	1.010	1.434	1.026	0.872	1.002	1.038	1.216	1.072	1.560
1.851	1.666	0.775	1.248	0.993	1.000	1.558	1.140	0.854	1.145
0.639	0.436	1.347	0.966	1.055	0.874	0.561	0.915	0.892	0.603
1.280	1.185	0.921	0.938	1.197	0.975	2.069	1.176	0.842	1.966

90	100	110	120	130	140	150	160	170	180	Baseline Density	Frequency from P & T
0.809	0.803	0.766	1.279	0.809	0.803	1.454	0.766	1.080	0.959	1.017	1.68866131
0.826	1.268	1.670	1.191	0.826	1.268	0.957	1.703	1.486	1.204	1.106	1.68866131
1.574	1.033	1.009	0.903	1.574	1.033	0.960	0.871	0.704	1.085	1.007	1.68866131

1.387	0.950	0.827	0.602	1.387	0.950	0.619	1.061	0.982	0.847	1.032	1.68866131
0.878	1.761	1.351	1.840	0.878	1.761	1.965	1.584	1.014	0.962	1.105	1.68866131
0.918	0.724	0.849	0.701	0.918	0.724	1.078	0.841	0.942	1.775	1.156	1.68866131
1.658	1.506	1.583	1.925	1.658	1.506	1.370	1.056	1.418	0.866	1.244	1.68866131
1.587	1.210	1.235	1.036	1.587	1.210	1.196	1.390	1.945	1.364	1.474	1.68866131
1.172	1.553	1.814	1.528	1.172	1.553	1.176	1.604	1.255	1.923	1.332	1.68866131
1.746	1.444	1.306	1.401	1.746	1.444	1.286	1.678	1.900	1.518	1.596	1.68866131
1.279	1.919	1.748	2.373	1.279	1.919	2.118	1.322	1.315	1.449	1.831	2.007278984
2.831	1.990	2.330	2.180	2.831	1.990	2.297	2.746	2.314	2.550	2.098	2.007278984
2.437	2.717	2.565	2.250	2.437	2.717	2.794	2.165	2.102	2.750	2.489	2.007278984
2.946	2.781	2.174	2.708	2.946	2.781	2.508	3.237	3.301	2.732	2.870	2.474585006
3.273	3.342	4.228	3.894	3.273	3.342	3.960	3.756	4.155	3.285	3.479	2.474585006
4.241	4.326	4.365	3.840	4.241	4.326	4.143	3.975	3.864	3.733	4.124	3.226338304
5.441	5.299	4.842	5.170	5.441	5.299	5.072	4.799	5.221	5.338	4.959	4.635875926
5.261	5.616	5.836	5.695	5.261	5.616	5.380	5.680	5.314	5.373	5.608	4.635875926

6.670	6.522	6.212	6.390	6.670	6.522	6.437	6.709	6.589	6.998	6.713	4.635875926
4.882	5.060	5.332	5.475	4.882	5.060	5.065	4.942	4.924	5.214	5.084	3.226338304
5.143	5.101	4.897	4.833	5.143	5.101	5.272	5.003	5.300	4.778	4.987	3.226338304
4.007	4.116	4.008	4.028	4.007	4.116	4.011	3.891	3.898	4.208	4.139	2.474585006
3.369	3.045	3.202	3.495	3.369	3.045	3.173	3.486	3.148	3.351	3.264	2.474585006
2.533	2.679	2.497	2.526	2.533	2.679	2.684	2.589	2.893	2.557	2.639	2.007278984
2.298	2.121	2.503	2.336	2.298	2.121	2.175	2.416	2.110	2.228	2.182	2.007278984
1.400	1.264	1.146	1.295	1.400	1.264	1.430	1.209	1.194	1.291	1.304	2.007278984
1.969	2.204	1.834	1.626	1.969	2.204	1.726	1.818	1.930	1.764	1.726	1.68866131
0.816	1.170	1.250	1.405	0.816	1.170	1.207	1.476	1.019	1.209	1.435	1.68866131
2.468	2.049	2.234	2.191	2.468	2.049	1.922	1.647	2.681	1.883	1.817	1.68866131
1.221	1.108	1.069	0.786	1.221	1.108	1.561	1.276	1.126	1.104	1.216	1.68866131
1.076	0.872	1.111	1.682	1.076	0.872	0.918	0.952	1.534	1.301	1.184	1.68866131
1.259	1.202	1.330	0.795	1.259	1.202	1.119	0.932	0.750	0.981	1.078	1.68866131
1.063	1.231	1.104	0.813	1.063	1.231	1.310	1.793	1.309	1.005	1.086	1.68866131

1.010	1.480	1.220	1.560	1.010	1.480	0.975	0.872	0.850	1.038	1.119	1.68866131
1.666	1.130	0.780	1.145	1.666	1.130	0.713	0.993	1.422	1.558	0.950	1.68866131
0.436	0.455	1.305	0.603	0.436	0.455	1.420	1.055	0.860	0.561	0.981	1.68866131
1.185	1.252	1.088	1.966	1.185	1.252	0.612	1.197	0.797	2.069	1.129	1.68866131

James Hunsucker (Student)	4/28/16 (date)
(Committee Chair)	4/28/16 (date)
(Committee Member)	4/28/2016 (date)
(Committee Member)	4/28/2016 (date)